JOHANN WOLFGANG GOETHE
UNIVERSITÄT
FRANKFURT AM MAIN

MAX-PLANCK-INSTITUT
FÜR POLYMERFORSCHUNG

Frankfurt am Main, 27.10.2016

Master Thesis

Kathrin Stadelmann
Student number: 5165416

Degradation study of lead sulfide quantum dots as sensitizer for solar cells (QDSSCs) with enhanced-Raman spectroscopy

Johann Wolfgang Goethe University, Frankfurt am Main Faculty of biochemistry, chemistry and pharmacy Institute of physical and theoretical chemistry

Max-Planck-Institute for Polymer research, Mainz

Research group Raman at Solid / Liquid Interfaces

Supervisor: Dr. Katrin F. Domke (MPIP Mainz)
First reviewer: PD Dr. Markus Braun
Second reviewer: Prof Dr. Josef Wachtveitl

Table of Contents

Abstract

The confinement of global warming to 2 °C is one of the most challenging tasks in the 21st century. The current research and development is dealing with a broad range of new concepts to solve this problem.[1] One approach is a solar cell based on quantum dots (QDs). Small bandgap lead chalcogenide QDs are used as an absorber for sunlight in QD sensitized solar cells (QDSSCs).[2] This offers a promising application, due to the absorbed sunlight in a broad range of wavelengths from UV to IR. Even in a region where photoactive materials are rare. In addition, QDSSCs have a size-tunable band gap that enables narrow emission bands. Furthermore, the manufacturing process is advantageous due to a simple and cheap solution process that reduces the cost significantly.

At present, devices with efficiencies of ~ 9% are obtained due to their strong affinity to oxygen, humidity and photothermal oxidation, which limits the efficiency and therefore the use in world market. Despite the importance of the degradation behavior, the details of the degradation are not fully understood.

The aim of this thesis is to characterize the degradation signature from lead sulfide (PbS) quantum dots with enhanced Raman techniques. Three samples were analyzed, that differs in the level of degradation. All samples were produced under inert conditions which include less than 0.011 ppm humidity and an oxygen level between 0.5 to 4.5 ppm. The evaluation of the measured samples in an inert and ambient atmosphere indicated photo-oxidation marker. For the analysis of the Raman signature, a technique with high chemical selectivity is necessary. Therefore, surface-enhanced Raman scattering (SERS) and tip-enhanced Raman scattering (TERS) were chosen. The presented study is important to gain information of PbS QDs behavior to improve the efficiency in photovoltaic applications.

Keywords:

Surface-enhanced Raman spectroscopy (SERS), Tip-enhanced Raman spectroscopy (TERS), Lead sulfide (PbS), Quantum dot (QD), Successive ionic layer adsorption and reaction, Degradation

Zusammenfassung

Die Begrenzung der globalen Erwärmung auf 2 °C ist eine der herausforderndsten Aufgaben des 21. Jahrhunderts. Die aktuelle Forschung und Entwicklung untersucht zahlreiche verschiedenen Konzepte, um dieses Problem zu lösen.[1] Eine Möglichkeit ist eine Solarzelle, die auf einem System aus Quantenpunkten (QP) basiert. Die Blei-Chalkogenide werden als Absorptionsmaterial für das Sonnenlicht in QP sensitiven Solarzellen (QDSSCs) verwendet.[2] Dies eröffnet eine vielversprechende Anwendung da sie einen sehr großen Bereich des Sonnenspektrums absorbieren können vom UV bis in den IR Bereich. Sogar in den Absorptionsbereichen in denen es wenig photoaktive Materialen gibt. Zusätzlich besitzen sie eine größenabhängige Bandlücke, die schmale Emissionsbanden ermöglicht. Des Weiteren ist die Herstellung sehr vielversprechend, da es sich um einfache und günstige Lösungsprozesse handelt, womit die Kosten signifikant reduziert werden können.

Derzeit werden Geräte mit einem Wirkungsgrad von ~ 9% erreicht. Dies liegt unter anderem an der starken Affinität der QP für Sauerstoff, (Luft)-feuchtigkeit und photothermischer Oxidation. Diese Limitation schränkt die Verwendung auf dem Weltmarkt stark ein. Daher ist es wichtig das Abbauverhalten zu untersuchen, da es noch nicht vollständig verstanden worden ist. Durch ein besseres Verständnis könnten die limitierenden Schwachstellen analysiert werden, um dadurch die Leistung, einer auf Quantenpunkt basierenden Solarzelle zu erhöhen.

Diese Arbeit basiert auf der chemischen Charakterisierung des Abbauprozesses von Bleisulfid (PbS) Quantenpunkten mit Hilfe einer signalverstärkten Raman Spektroskopie. Es wurden drei verschiedenen PbS QP Proben untersucht, die sich in ihrem Abbaugrad unterscheiden. Alle Proben wurden hergestellt unter inerten Bedingungen. Dies beinhaltet weniger als 0,011 ppm (Luft)-feuchtigkeit und einem Sauerstoffniveau zwischen 0,5 – 4,5 ppm. Der Vergleich zwischen nicht degradierten und degradierten Proben zeigt Photooxidationsmarker auf. Um die Signatur analysieren zu können, musste ein hochsensitives Verfahren mit einer hohen chemischen Selektivität gewählt werden. Für eine optimale Verstärkung der gemessenen Raman Streuung wurden die Methoden der oberflächenverstärkten Raman Spektroskopie (SERS) und der spitzenverstärkten Raman Spektroskopie (TERS) verwendet. Die

gezeigte Untersuchung ist wichtig für ein besseres Verständnis der PbS QP, um die Effizienz photovoltaischen Anlagen zu verbessern.

Schlüsselwörter:

Oberflächenverstärkte Raman Spektroskopie (SERS), Spitzenverstärkte Raman Spektroskopie (TERS), Bleisulfid (PbS), Quantenpunkt (QP), Aufeinanderfolgende Schichtadsorption und Reaktion, Abbau

List of abbreviations

AFM	atomic force microscopy
EC	electrochemical
EDX	energy dispersive X-ray spectroscopy
EF	enhancement factor
EM	electromagnetic
LSP	localized surface plasmons
LSPP	localized surface plasmon polariton
IR	infrared
PbS	lead sulfide
PV	photovoltaic
QCE	quantum confinement efficiency
QDs	quantum dots
QDSSCs	quantum dot sensitized solar cells
SC	solar cells
SEM	scanning electron microscopy
SER	surface-enhanced Raman
SERS	surface-enhanced Raman spectroscopy
Si	silicon
SILAR	successive ionic layer adsorption and reaction

SP	surface plasmons
STM	scanning tunneling microscopy
TER	tip-enhanced Raman
TERS	tip-enhanced Raman spectroscopy
UV	ultraviolet
Vis	visible

List of symbols

α	polarity
Å	Ångström
a_B	exciton Bohr radius
c	speed of light
ΔE	energy difference
e	permittivity
ε	dielectric constant
E_g	bandgap
E_{tip}	enhanced electric field under the tip
E_0	incident electric field intensity
g	enhancement
$h\nu_{in}$	energy of incident photon
$h\nu_{sc}$	energy of scattered photon
$h_{\Delta\nu}$	frequency loss
I_{in}	intensity of incident photon
I_{sc}	intensity of scattered photon
k	wave vector
μ_{ind}	induced dipole moment
R_p	particle radius
σ	Raman cross section

T	absolute temperature
ν_{in}	incident wavenumber
ν_G	vibrational level
ν_{sc}	scattered wavenumber
υ_0	Rayleigh-scattering
λ	wavelength
s	second

1 Introduction

The energy demands are getting higher and the need to find a solution is increasingly strong. A source of clean energy is sunlight, since the sun is a constant source of blackbody radiation at 5.800 K. On a daily basis approximately 9 x 10^{22} J of energy reaches the Earth. The daily consumption by human activity is about 9 x 10^{18} J.[3] Therefore, a considerable interest in solar cells (SC) is discernible for years. The solar cells convert sunlight into electricity through the photovoltaic (PV) effect[4] by using conventional solar cells which are based on silicon (Si). However, high production costs due to sophisticated manufacturing[5] and the incapability to use the whole solar spectrum[6] are the main reasons to investigate new materials for SC technologies.

The new candidates for SC are small band gap QDs. QDs are becoming attractive for photovoltaic and optoelectronic applications due to the tunable bandgap that enables a broad range of wavelengths absorption[7–11] from the UV to the IR (750 to 2400 nm).[12,13]

Until now, the efficiency of QD solar cells has not reached the efficiency of silicon solar cells. One reason for their reduced efficiency is their affinity to oxygen and humidity and which results in fast degradation through the formation of oxidation products. In order to improve the efficiency, a detailed understanding of the degradation behavior is essential. Studies to understand the degradation behavior could lead to answering the following questions: Which oxidation products exist, what is their contribution and furthermore when and how fast the degradation happened? Answering the questions would allow an improvement of QD solar cells based device performance. Consequently, the lack to understand the degradation behavior of PbS QDs leads to an exploration of methods in the last decade[14–18] to avoid the degradation process, such as encapsulation,[19] passivation[20] or functionalization.[21] However, this thesis is a trial to understand the degradation behavior of PbS QDs.

The degradation behavior of PbS QDs is studied with three types of samples. The PbS QDs samples were fabricated under nitrogen atmosphere and were measured in atmospheres with different oxygen contents. The main concern of this study is to characterize specific oxidation markers that are linked to the degree of oxidation.

Conventional Raman technique need high excitation power[22,23] and/or long integration time to detect a signal of a low concentrated sampel.[24,25] But high excitation power (40 mW) and/or long integration times (10-15 min) induce sample damage. The degradation of PbS QDs was monitored with surface-enhanced Raman spectroscopy (SERS) and tip-enhanced Raman spectroscopy (TERS). Both of those techniques are highly sensitive and chemically selective techniques due to the enhancement of the Raman scattered signal. Thus, the Raman signature of PbS QDs (sub)-monolayer can be recorded with low power (0.15 mW) and short integrations times (10 s). Rough metal surfaces enhance the electromagnetic field and overcomes the drawback of low Raman cross section.

2 State of the Art

2.1 Raman spectroscopy

2.1.1 Raman effect

The phenomenon of inelastic light scattering was postulated by Smekal in 1923 and first experimentally realized by the Indian physicist C.V. Raman in 1928.[26] When induced light illuminates a molecule radiated scattered photons can be obtained. When the scattered photons have a frequency shift in comparison to the incident photons it is referred to as Raman effect.[27] The Raman technique is based for the inelastic scattering of photons while other technique, like IR spectroscopy, is based on the absorption of photon(s). Raman spectroscopy is a useful tool to gain the vibrational information of gas, liquids or solids.

In the visible region the wavelength of light (400 - 700 nm) is quite large in comparison to the diameter (0.32 nm) of a carbon dioxide molecule.[28] If the incident electromagnetic (EM) wave excites the molecule, the electron cloud is perturbed periodically with the same frequency and the electrons follow the EM field. Therefore, polarizability is necessary. The polarizability describes how easy electrons can move in response to an oscillating electric field. The oscillation of the electron cloud is much faster than the motion of the heavy nucleus and therefore the nucleus cannot follow the induced oscillation. The dynamical response of the molecule to the external field leads to a charge separation in the positive nucleus and the negative electron cloud. The separation of charge is referred to as induced dipole moment μ_{ind}.[27] The change in the polarizability of the electron cloud is the requirement to induce a dipole moment in the molecule. The strength of the induced dipole depends on the polarizability tensor, α, and on the electric field, E. Following the equation (2.1):[29]

$$\mu_{ind} = \alpha \cdot \mathrm{E} \qquad (2.1)$$

The scattering phenomenon is illustrated in the schematic energy diagram, shown in Figure 2-1. The light interaction with the molecule leads to a *"short-lived state"*, which is referred to as *"virtual energy level"*. The *"virtual energy level"* is not a real state; it

is used to explain the mathematics and is helpful to image the Raman scattering process. Light can be considered as a stream of photons. When the photons interact with the molecule three different ways of scattering will be detected. The majority of the induced light are elastically scattered in a process known as Rayleigh scattering. As pictured in Figure 2-1b, the energy of the incident photon, $h\nu_{in}$, and the scattered photon, $h\nu_{sc}$, is equal. During the Rayleigh process the molecule relaxes down to the ground state without a transfer of energy.

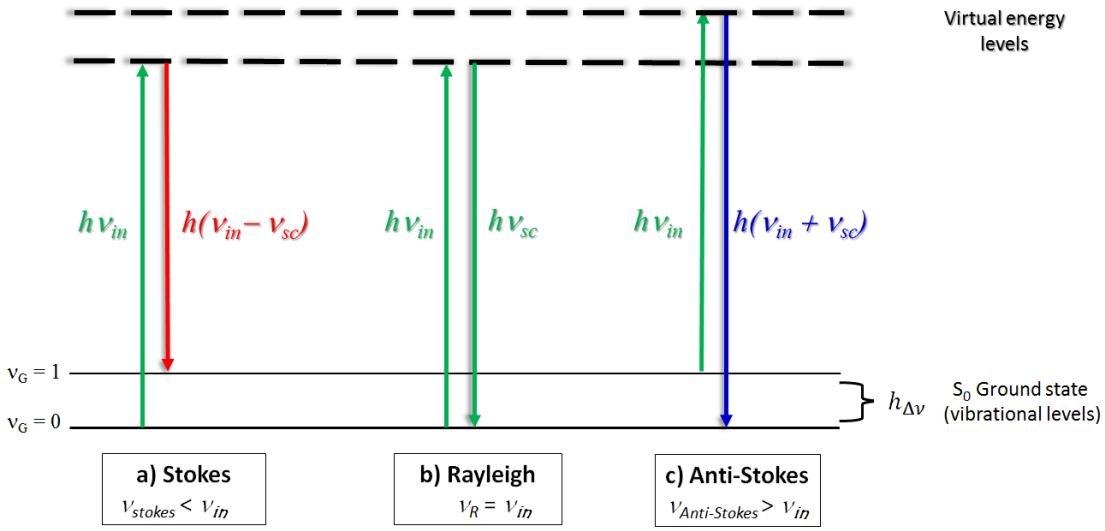

Figure 2-1: Schematic of the Rama effect. Frequency and energy of the incident photon ($h\nu_{in}$) are transferred to the molecule. Three different ways of scattering will happen during the emitting of the "*virtual energy level"* in the *ground vibrational level* ν_G The scattered photon ($h\nu_{sc}$) has a lower frequency (a, Stokes, red-shift), the same frequency (b, Rayleigh) or a higher frequency (c, anti-Stokes, blue-shift) than the incident photon**.**

The processes of interest for Raman measuring are the inelastic scattered processes, known as Stokes and anti-Stokes scattering. Since, an energy transfer between the incident light and the molecule occurs which results in two different scattered frequencies. During the Stokes scattering (Figure 2-1a) the molecular vibrations are excited from the vibrational levels $\nu_G = 0$ in the *"virtual energy level"* and return immediately to a higher vibrational level $\nu_G = 1$. Therefore, a photon with less energy than the incident photon is emitted.[27] The photon is recorded with the frequency

difference $h_{\Delta\nu}$ and results in a red shift of the Raman spectrum, due to the frequency lost $h(\nu_{in} - \nu_{sc})$.[27]

The second scattering process occurs if the molecule is already in a higher vibrational level, for example at $\nu_G = 1$ instead $\nu_G = 0$. The incident light excites the molecular vibration from $\nu_G = 1$ to higher *"virtual energy level"* and returns immediately back in the vibrational ground level $\nu_G = 0$. The emitted photon gains energy and emits a photon with higher frequency $h(\nu_{in} + \nu_{sc})$ in comparison with the incident photon. This process is referred to as anti-Stokes scattering (Figure 2-1c), and leads to a blue shift in the spectra.[27] The distribution of the inelastic scattering in Stokes and anti-Stokes scattering depends on Maxwell-Boltzmann population, which means it depends highly from temperature. Following the population in the ground state at room temperature is much higher than in excited states. In consequence of the inefficiency of the anti-Stokes scattering the intense Stokes scattering is mostly used for experiments. In summary, the polarizability of the electron cloud around the molecule will follow the electric field of the incident light. The differences in the vibrational level correspond to a shifted frequency, which is detected as a scattering and give the vibrational spectrum.

2.1.2 Raman cross section

Raman scattering is actually a very weak process of second order in comparison to the Rayleigh scattering or fluorescence signals. Only one of 10^{-8} - 10^{-6} photons of incident radiation undergoes a spontaneous Raman scattering.[30] Therefore, values for Raman scattering are very low, ~ 10^{-31} - 10^{-29}.[31] Which means a very high concentrated sample or/and a very long intergradation time is necessary to get a good Raman spectrum. The Raman cross section is defined as the ratio between the intensity of scattered radiation (I_{sc}) and the intensity of the incident wave (I_{in}), see equation (2.2):[32,33]

$$\sigma = \frac{I_{sc}}{I_{in}} \qquad (2.2)$$

The low Raman cross section limits the applications of this advantageous Raman technique and Raman was used for long time just for "bulk" materials. The instrumentation progresses, including the development of the laser in the 1960´s and the

improvement of the sensitivity of detectors improved highly the Raman intensity. As a result, the Raman technique moved back into the laboratories.[26]

But not all molecule vibrations are Raman active and can be detected. The next section gives a brief introduction which vibrations are Raman active using the Raman selection rules.

2.1.3 Raman selection rules

The total of normal modes for a molecule with N atoms can be calculated with the equation 3N-6 for non-linear molecules and 3N-5 for linear molecules.[27] These formulas include three degree of freedom, which describes the translation and three degrees of freedom, which describe the rotational movement (for linear molecules two degrees of freedom) of the molecule. In order for a molecule to be Raman active it must have a change in its polarizability. A high polarizability leads to a high scattering. This means, a change in the size, shape or orientation of the electron cloud is necessary. Usually, the changes occur in symmetric stretching but not in asymmetric stretching. In the next section some points are explained which are useful for the interpretation of a Raman spectrum.

2.1.4 Raman spectrum

In Raman spectroscopy, wavenumbers in cm^{-1} are used to characterize the scattered photon energy. The Raman signals are characterizing with the Raman shift. The Raman shift is the energy difference, ΔE, between the incident radiation and the Raman scattered radiation. The Raman shift is calculated with the following equation (2.3):

$$\Delta E = \frac{1}{\lambda_{in}} - \frac{1}{\lambda_{sc}} \qquad (2.3)$$

The Raman vibrational fingerprint can be roughly divided in approximation areas. Raman vibrations in the area of 0 to 500 cm^{-1} include mostly heavy atoms. The range from 500 to 1800 cm^{-1} is interesting for biology systems. The range between 1800 to 2800 cm^{-1} involves less vibrations and overtones, mostly alkyne vibrations. Finally, in the range between 2800 to 3500 cm^{-1} lightly molecules such as CH_2 can be detected. To characterize a Raman spectrum, it is useful to pay attention to following facts. The peak position depends on the environment and energy level of the scattering

vibrations.[27] The dynamics of the molecule, like motion can be analyze from the *full with half maximum* (FWHM), if the peak is not an overlay of different vibrations.[27] The Raman intensity is influenced by a number of reasons, such as the number of molecules, the laser intensity - and wavelength. Due to all these variations, it is common to use the "*relative intensity"* instead of the "*absolute intensity"* for peak characterization to compare the peaks between different spectra. The "*absolute intensity"* is the actual intensity which is detected. The "*relative intensity"* is the comparison of one peak relative to another peak in the same spectrum. This means, the counts of the detected intensity of a spectrum are not used for comparison between spectra. The comparable results are achieved with the analysis of "*relative intensities"*. In non-conventional Raman techniques, a strong Raman background can exist. The background depends on the used Raman technique and on the chosen sample. The background correction depends also on the measurement, sometimes the background includes information and therefore the background will not be subtracted. More information on the Raman background can be found in the article of Pilz and Kriegsmann.[34]

The Raman signal from a low amount of adsorbed molecules, like (sub)-monolayers, is impossible to detect with the conventional Raman technique. Raman techniques have been developed to enhance the Raman signal. In the next chapter a way to enhance the intensity of Raman signals is discussed which is based on the electromagnetic enhancement of localized surface plasmons.

2.2 Enhancement of the electromagnetic field

In this chapter the enhancement of the EM field is discussed which is based on the localized surface plasmon (LSP). The discovery of the enhanced Raman technique makes it possible to enhance the weak Raman cross section.[29] Metals, like gold, silver or copper are widely used since their optical response is resonant with the incident EM wave of the visible light. The next section describes the enhancement effect and the quasiparticles which are necessary for the enhancement of the EM field.

Plasmons are *quasi-particles* representing the modes of charge density oscillations. In other words, collective excitations of electrons in metals leading to plasma oscillations with respect to the ionic cores of plasmons.[29,35]

Plasmons are referred to as surface plasmons (SP) if they are close to the interface between the metal surface and dielectric (air). At the interface SP are maximal and the longitudinal electronic vibrations (SP) are excited parallel to the metal surface, see Figure 2-2a. The propagating of the SP along the metal surface is limited by the transformation of the SP vibration energy in thermal energy. The propagation of SP depends strongly on the chosen material, for example, 9 micron for gold and 100 micron for silver. In the perpendicular direction the intensity of SP decays exponentially with distance from the interface (Figure 2-2b). The non-radiative decay in metals is responsible for the transformation of plasmon vibrational energy into thermal energy.

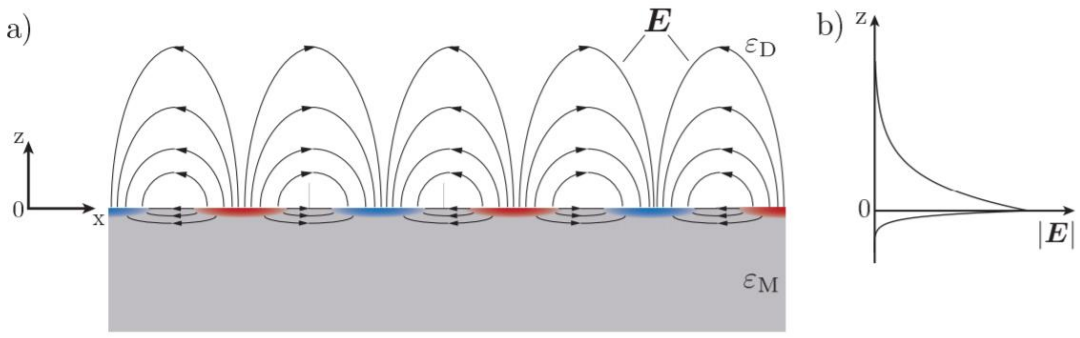

Figure 2-2: a) schematic of propagate surface plasmons in x-direction at the interface between the metal and the dielectric. Areas with higher or lower areas are blue or red coloured. b) The penetration depth in the dielectric is stronger than in the metal. and dielectric. The intensity of SP decays exponentially with distance from the interface.[36]

For the excitation of SP by the incident EM wave the momentum conservation have to be fulfilled.[33] The difficulty is the SP cannot be excited by an incident radiation frequency in a smooth metal surface due to the wave vector and momentum mismatch of the incident photon with the wave vector and the momentum of the SP.[27,29,36] This means SP are not able to radiate in the dielectric nor be excited by incident radiation. If we are imagining the dispersion curve is it necessary does the incident light intercept with the surface plasmons to excite the SP.[37] Therefore, the energy and momentum conservation of both have to be fulfilled. But the wave vector of the SP are always larger as the wave vector of incident light.[36,33] Techniques are developed to increase the wave vector of the incident EM wave with optics, such as prism or grating.[29] With

momentum-matching techniques like this is it possible to create a wave vector and momentum matching.

Due to the nanostructuring, which works as a "gab" the SP modes lose their propagating nature and are localized.[33] The spatial trapped localized SP at nanostructures on the metal surface is referred to as localized surface plasmon (LSP). The LSP is a standing wave (evanescent wave).[29] This means the LSP is effectively trapped at the nanostructured metal surface and does not propagate.

Nanostructuring enables the coupling of the incident EM wave with LSP mode. If the dimension of the nanostructured material ($\emptyset$) is smaller than the incident wavelength $\emptyset \ll \nu_{in}$. The momentum and wave vector matching enables the excitation of LSP due to the EM wave, when the LSP are in resonance with the incident EM wave.[37] The resonant coupling of the LSP with the incident EM wave leads to localized surface plasmon polaritons (LSPP), which are oscillate. The evanescent wave creates an immensely strong electric field.[29] The strong near-field leads to vibrations in the adsorbed molecule after the excitation with the incident EM wave (vibrational process was described in 2.1.1). After the relaxation of the molecule the near-field information is transferred into far-field information and those propagating waves can be detected as strong enhanced far-field signal. The enhancement is a result of the local enhancement of the incident EM wave at a rough metal surface which maximize the incoming and the outcoming radiation.[29]

To summarize, LSPP are the important modes that are used to enhanced the EM field. Without the strong enhancement of those fields it would not be possible to detect weak signals.[29] The strong field enhancement of the near-field opened new applications. Information received from the evanescent field overcomes the limitation of spatial resolution and imaging of nanostructures are possible, which could be used for surface studies.[29,35,37] One special technique, which uses the enhancement of the near-field through LSPR, is the powerful surface-enhanced Raman spectroscopy (SERS) method, which will be discussed in the next chapter.

2.3 Surface-enhanced Raman spectroscopy on rough metal surfaces

Surface-enhanced Raman spectroscopy (SERS) overcomes the limitation of Raman low cross section by the combination of Raman spectroscopy with nanostructured metal surfaces. SERS is highly specific, which provides a unique vibrational fingerprint of an ensemble of adsorbed molecules on the SERS substrate surface. The high sensitivity and the short intergradation time even with low concentrations make the method so useful for the study of (sub)-monolayers. The polarized molecule can be measured directly without any additional steps, like staining. Figure 2-3 illustrate an example between the enhanced and the conventional Raman spectrum on the sample of the dye Rhodamine 6G.

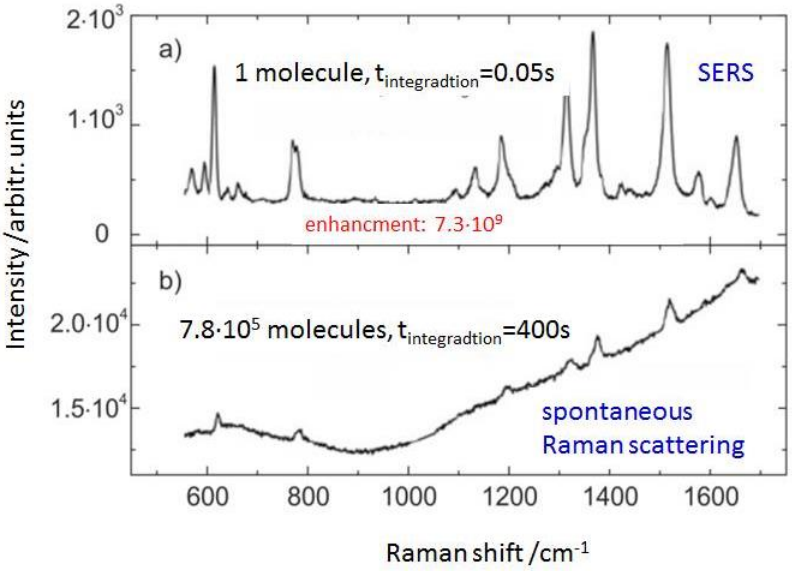

Figure 2-3: a) SERS spectrum of a single dye Rhodamine 6G in the near-field with an integration time of 0.05 s. b) conventional Raman spectrum of Rhodamine 6G in water (100µM, approx. $7.8 \cdot 10^5$ molecules in the focus) and a integration time of 400s. Both spectra were detected with an excitation of λ_{ex}= 632.8 nm, a laser power of 3 mW and a 100x oil-immersion objective. In comparison to the clear peaks of the SERS spectrum, is the detection with the conventional Raman spectrum limited to the peaks with the highest intensity in Raman-resonance. All the other peaks in the non-enhanced Raman spectrum are not detectable due to the fluorescent background.[38]

A single dye molecule on the nanostructured metal surface gives an enhanced Raman signal with a factor of $7.3 \cdot 10^9$ in comparison with a water dissolved Rhodamine 6G solution (100µM, approx. $7.8 \cdot 10^5$ molecules).[38] The SERS effect was first reported by Fleischman et al. in 1974[39] and the surface-enhanced Raman effect was correctly explained independently by Van Duyne et al. and Jeanmaire et al. in 1977.[40] After 40 years the physical mechanisms of SERS are still discussed controversially. The enhancement mechanism is a result of the locally plasmon induced near-field superelevation, referred to as EM enhancement. In the following section the enhancement based on the EM factor is introduced in relation to the SERS technique.

2.3.1 Enhancement effect of SERS

The basics of the EM enhancement theory were explained in chapter 2.2. The idea of SERS is the coupling of incident light with LSP on a rough surface which leads to huge EM fields and a huge scattered Raman signal is achieved. Therefore, SERS is based on the local excitation of surface plasmons and the resonance of those with the EM wave. Due to the relaxation of the momentum conservation the excitation of LSP with EM wave is possible. The rough surface allows an excitation of localized surface plasmons with the incident light, which leads to locally huge enhanced electromagnetic fields, see Figure 2-4.

SERS works only with a few noble metals, such as gold (Au), silver (Ag) and copper (Cu). Those metals lie in the resonance area with the wavelength of the visible light. Consequently, the SERS enhancement depends on the quality of SERS substrates, rough metallic nanostructured substrates are needed.

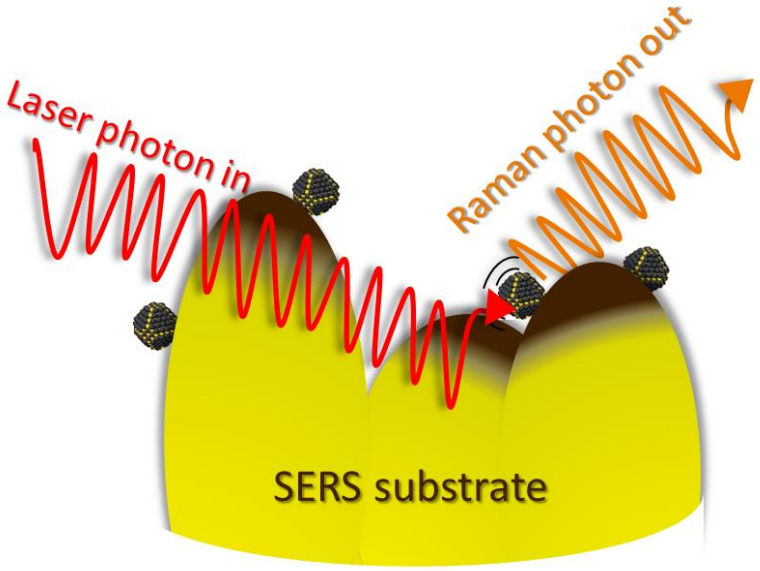

Figure 2-4: Schematic of the excitation of localized surface plasmons through an incident EM wave on a nanostructured metal surface (SERS substrate) which leads to strong enhancement of the scattered Raman signal.

In addition, there is another enhancement mechanism, which is denoted as chemical enhancement.[41] If the molecule builds a chemical bond complex with the surface it can enhance the signal by 10^2.[37] For example, the Raman enhancement for water is less enhanced than the enhancement for lead sulfide. Therefore, the order of the total enhancement also depends on the type of adsorbate. The chemical enhancement is quite less in comparison to the electromagnetic enhancement factor. Further, there is a first layer effect.[37] Directly, adsorbed molecules on the SERS surface received a larger enhancement effect than additional layers by orders of magnitude. In total the SER enhancement factor is the product of the long-range electromagnetic and the short-range chemical contribution. Total enhancement factors of 10^6 or higher has been observed.[37]

The intensity of conventional Raman spectroscopy scales linearly with the intensity of the incident electromagnetic wave. For the enhanced Raman technique, a factor of $|E^4|$ is obtained due to the $|E^2|$ dependency of the electromagnetic fields from the incident radiation and the scattered Raman radiation.

The enhancement of the EM field is not homogenous on the entire sample surface. On every SERS substrate there are small areas on the rough surface structure which produce specific highly localized points with a huge SERS enhancement. Only very few spots support intense Stokes scattering of the adsorbate, which are referred to as *"hot spots"*.[37] "Hot spots" are highly spatially localized regions, which are responsible for the extreme enhancement of Raman scattering. If the adsorbate is adsorbed in the gap between two nanostructures or nanostructured agglomerates, an extreme enhanced field is produced.[29] The shorter the distance of two nanostructures in the near-field the better the "hot spot" enhancement. Therefore, "hot spots" are the perfect location for a target molecule.[37] But the probability of finding a molecule in the gap between nanostructures is very small. Most of the molecules adsorb at positions on the SERS surface with moderate enhancement factors.[37]

The next section introduce SERS substrates due to the quality of the SERS substrates influences strongly the information of the scattered Raman signal.

2.3.2 SERS substrate

The rough metal surface, which is based on the structure size, geometry, distance between two nanostructures and the spatial arrangement of the nanostructure are immensely important for a SERS substrate. The Raman intensity depends strongly on the optical properties of the SERS substrate. Au and Ag have optimal optical properties to sustain high plasmon resonance in the interesting range. All those details effect the enhancement of the local EM field. The nanostructure is created by controlled nano-fabrication, like etching or evaporation processes.[42]

Researchers have developed and are still developing new nanostructures that generate a lot of homogenous and reproducible *"hot spots"* to enhance the LSPR. The newest designed nanostructures can achieve large local field enhancement. Some points categorize a good SERS substrate; the achievement of a good stability and reproducibility between different substrates of the same substrate type. Also, a uniform enhancement on the substrate is needed for the characterization. The ability to apply different adsorbates efficiently on individual substrates is advantageous. If the molecules do not adsorb efficiently on the surface the SERS enhancement is low. For a

high Raman intensity also the SER probe is important. The excellent candidate for a strong plasmon resonance should efficiently adsorb close to the surface to receive a very huge enhancement.[43]Also the orientation of the molecule relative to the surface is important and influence the signal of the SERS signature. For example, vibrational bands of an aromatic compound are differently enhanced if it is tilted, perpendicular or flat adsorbed on the SERS surface due to in-plane and out-of-plane modes. Finally, a strong SERS activity leads to a high sensitivity. Some SERS substrates provide less enhancement variations than other SERS substrates. Enhanced nanostructures could be colloidal solution or nanopillars.[42] Hot spots are also created on sharp edges, like inverse pyramids.[37]

In this thesis silicon needles (pillars) coated with gold are used as SERS substrate. At nanopillar substrates the scattered signal is strongly influenced by the molecule position. The strongest SER signal at nanopillar structured surface can be detected in a pre-leaned (Figure 2-5B) and in the post-leaned formation (Figure 2-5C).[42] Whereby, the post-leaned effect is stronger than the pre-leaned effect due to the both near-fields around the adsorbate.

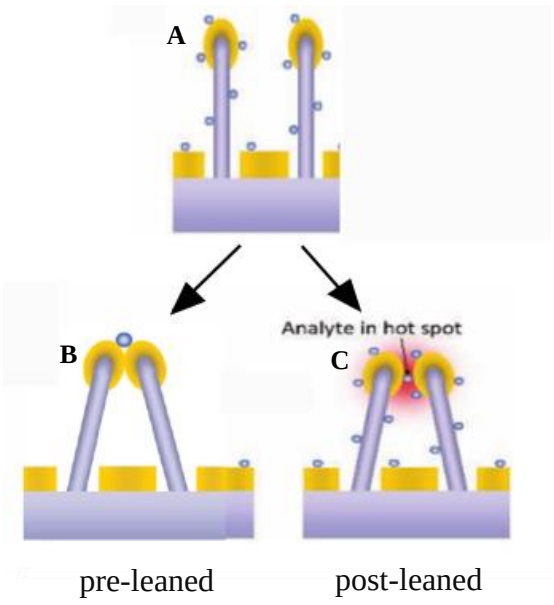

Figure 2-5: A) The schematic shows different possibilities of the signal enhancement. At the beginning the solvent is adsorbed on and between the nanopillar-structured surface. When the solvent is evaporated, surface tension can pull the pillars together in two different ways B) the pre-leaned state or C) the post-leaned state. The post-leaned state create a huge field enhancement due to the creation of "*hot spots"*.[42]

The perfect SERS substrate was not found until now. Up to now it is still in discussion which substrate geometry produces the most intense field enhancement. A problem of the SER experiment is the signal variation due to SERS substrate geometry, orientation and strength of the adsorbed adsorbate. The difficulties in the SER measurement are discussed in the next chapter.

2.3.3 Problems of SERS substrate

SER enhancement is influenced by a lot of different factors; the set-up, the laser excitation, the SERS substrate and the adsorption property of the adsorbate. All those variations make it nearly impossible to compare SERS results which were not recorded with the same set-up even if the same type of SERS substrate was used. The reproducibility can be achieved with an average of differently measured spots over the whole sample. The detected SER signal is a summary of the maximal enhanced SER signal and the average of differently strong enhanced SER signals. Measured SER signals of a sample can differ from signals measured with a conventional Raman due to the polarization dependency of plasmon resonances.[37] Meaning, the selection rules for Raman are no longer totally strict. It is possible to detect non-active or forbidden Raman modes. Also a broadening or a shift of the Raman signal can occur due to the creation of a surface complex.

SERS is a powerful tool which is easy to measure with a conventional Raman setup. Nowadays single-molecule measurements with SERS are possible but still complicated. SERS stuck to the nanostructured surface which involves problems for example, the difficulty in the reproducibility within SERS substrate. SERS creates *"hot spots"* and a variation of different enhancement factors spread over the whole SERS substrate which leads to different signal intensities. A new technique, the tip-enhanced Raman spectroscopy (TERS) overcomes the problem with the inhomogeneous signal enhancement and is explained in the next chapter.

2.4 STM-tip-enhanced Raman spectroscopy on smooth metal surfaces

In the last few decades researchers tried to overcome the drawbacks of SERS technique. Therefore, new ideas were developed to be independent from the roughness of noble metals. These limitations can be surmounted by employing a STM tip for local EM field enhancement. The metal-STM tip acts as the only "roughness factor" at smooth metal surface for enhanced Raman spectroscopy.[21] The advantage of TERS is the creation of only one single *"hot spot"* on the whole substrate. The *"hot spot"* can be create everywhere on the smooth metal substrate.

The first person to demonstrate the idea of TERS was Wessel et al. in 1985. In 2000, different groups Zenobi[44], Anderson[45] and Pettinger[29] independently reported the first tip-enhanced Raman results. The TERS set-up combines two powerful techniques. The Raman spectroscopy provides chemical information combined with a scanning probe device, such as STM or AFM which provides topographic information. The scanning probe device can work in contact or tunneling mode.[29,46] In this thesis the focus laid on the STM since this technique was used for TERS. TERS nano-imaging enables high spatial resolutions down to 1 - 10 nm with ultrahigh vacuum and/or low-temperature conditions. The high spatial resolution enables single-molecule detection and mapping on the sample. With the scan mode of STM interesting parts of the sample can be selected and the chemical information of those parts can be characterized afterwards with Raman spectroscopy.

As TER substrate noble flat metals are used, mostly Au and Ag evaporated /sputtered on a glass substrate. Smooth surfaces can be produced with an annealing process to avoid any structures on the surface. Structures on the metal substrate surface should be avoided due to the possibility of tip crashing and the creation of SER signals. The smooth metal substrate located below a STM tip and only the adsorbates underneath the tip apex are sin contact with the near-field and leads to an increased far-field of the Raman scattering.

To create the near-field it is necessary to focus the laser on the apex of the tip in the correct focus point. The focusing is quite delicate and requires a good training on the TERS set-up to create LSPR.

2.4.1 Enhancement of TERS

The localized enhanced EM field is induced by localized surface plasmons in the tip and the interaction of the propagating incident EM wave. The enhancement of TERS is created with the same physical principle of LSPP as in SERS substrates.[47] The EM wave (far-field) couples with the STM-tip and the near-field is generating with a smaller dimension than the incident wavelength, which enables a tremendous field enhancement. The illuminated tip in tunneling contact represents a "single hot spot" in comparison to the creation of a lot of *"hot spots"* via nanostructuring via SERS.

The tip, which includes the LSP, serves as nanoantenna for the incoming and outgoing EM wave. This means the incident EM wave, as a far-field, interacts with LSP on the STM gold tip and creates a near-field. To create the near-field the incident light with a size of 0.5 µm is focusing on the apex of the very sharp tip with a radius of 20 to 50 nm. This leads to a highly localized surfaced charge density (LSPP), see Figure 2-6. The localized energy is used to excite an adsorbate that is in the near-field. The excitation of the adsorbate leads to vibrations. After the relaxation of the adsorbate the free scattered Raman photons can be detected as enhanced EM wave (far-field). The STM tip acts as nanoantenna for the incident EM wave and for the enhanced scattered Raman signal.

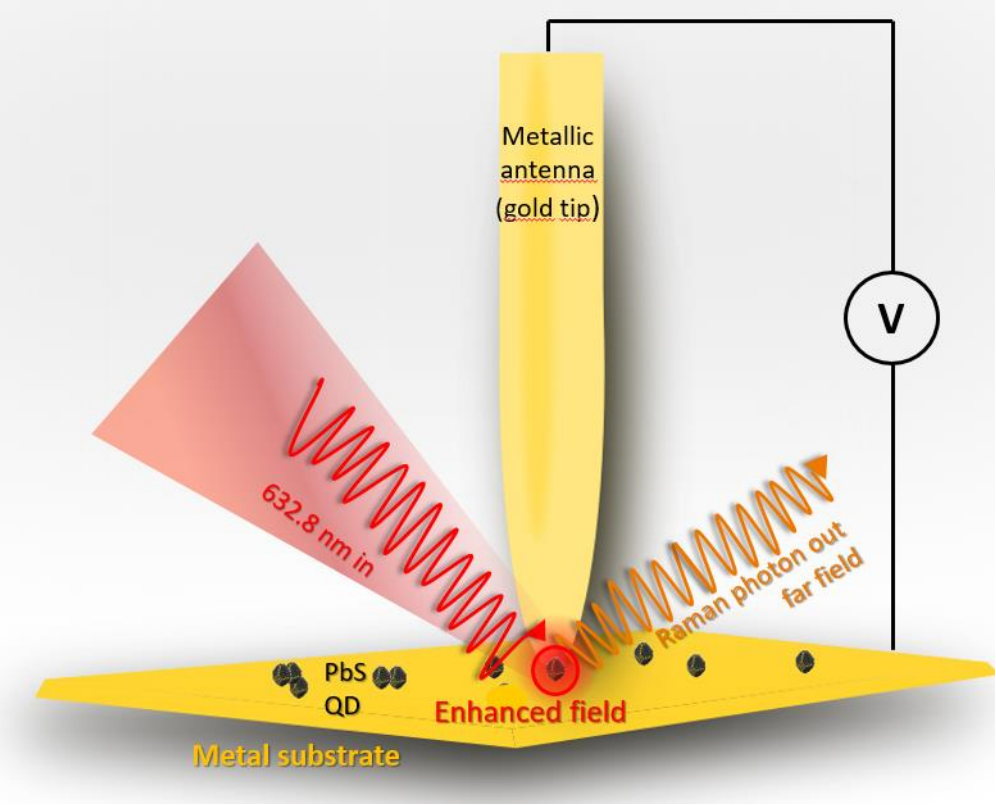

Figure 2-6: Schematic of the electromagnetic enhancement mechanism of tip-enhanced Raman scattering. The laser with a determined frequency is focused on the apex of the metal tip. The resonance of the laser with the localized surface plasmons in the STM-tip creates a strong field enhancement between the tip apex and the metal substrate which is called "*hot spot*". The "*hot spot*" experiences the strong enhancement of the electromagnetic field and the enhanced Raman scattered signal can be detected.

The excitation of LSP in the tip leads to high field enhancement in the vicinity of the tip apex by the tunneling tip. Therefore, it becomes very sensitive to the field distribution at the tip apex. The EM field enhancement is following the plasmon resonance of the tip, which works as nanoantenna and breaks locally the law of momentum conservation. A clear enhancement is observed if the tip is approached in the position of tunneling current. If the tip is retracted, no signal or a very weak signal is detected in comparison to the approached state.

The spatial resolution depends on the shape and size of the tip apex and can improve the limitation of the light beyond the diffraction limit. In a recent paper, Demming et al.[47] presented calculations of the field enhancement on illuminated scanning probe tips and

found maximal field enhancement factors at the apex of the tip, depending on its shape. The enhancement factor, EF, is a very important concept in TERS. The Raman enhancement, g, originates from the enhanced electric field under the tip, $E_{tip,}$ and the incident electric field intensity, E_0. The electric field enhancement g is calculated with the equation (2.4):[46]

$$g = \frac{E_{tip}}{E_0} \qquad (2.4)$$

The light intensity is proportional to the second power of field enhancement. The EF depends on the electric field enhancement of incident laser, g_{in}, and on the electric field enhancement of Raman scattering g_{sc}. The difference of the wavelength between the illuminating laser and the Raman scattering is less. Therefore, it can be assumed that the electric field enhancement of Raman scattering and laser is almost the same, if the Raman shift of both is not very large. The TERS enhancement factor can be calculated with the equation (2.5):[46]

$$EF_{TERS} = g_{in}^2 \cdot g_{sc}^2 \approx g^4 \qquad (2.5)$$

The enhancement of the Raman intensity scales with the 4^{th} power of the local EM field. Strong enhancement of the Raman signal combined with all advantages for high resolution imaging open new avenues towards single molecule Raman spectroscopy at smooth and crystalline surfaces. The development of the conventional Raman spectroscopy to TER-technique results in a powerful tool for fundamental solid-state research. This new technique enables surface scientist the characterization of sub-(monolayers) and new research fields, like electrochemical environment.

The description of the Raman setup is also helpful to understand the experiment. Therefore, the instrumentation is explained in the following chapter.

2.5 Instrumentation

The enhanced Raman signal is detected with a sophisticated set-up, which will be explained in detail. The reason for a thoughtful design of the set-up is the low Raman cross section.[27] Additionally, some materials have a tendency to degrade fast or bleach. Therefore, parameters such as high power and long intergradation time should be

avoided. To answer different research questions, the Raman set-up can be modified, but it always consists of the following main components: excitation source, monochromator, collection optics, filter and detector. In the following text some important components of the Raman set-up are explained.

Excitation source

The laser (light amplification by stimulated emission of radiation) enables monochromatic light with a specific frequency, due to the coherent (waves with same phase and direction) and collimated laser sources. The radiation is very strong and produces a high amount of photons with the same frequency.

Collection optics

An optical microscope is used in dependency of the set-up as long or short-distance working objective. The long-distance working objective in this thesis is used to irritate the sample with the laser source and to collect the randomly back-scattered Raman photons. The spatial resolution depends on the excited wavelength ν_{in} and the numerical aperture, NA, of the objective. The Abbe limit gives the smallest possible distance, Δx, between two separated objects, equation (2.6):[46]

$$\Delta x = \frac{0.61\,\lambda}{NA} \qquad (2.6)$$

Filter

The filter blocks specific wavelengths. Different types of filter fulfil different duties. For example, edge filter cut off the stray light and the Raman scattering.

Detector

With the technology revolution of the new generation of detectors more sensitive and shorter acquisition time are necessary in comparison to the forerunners, which leads to a huge quality improvement of the detected Raman signal. The charge coupled device (CCD) detector is mostly used and converts light in electrical signal.

Scanning tunneling microscopy (STM)

The scanning tunneling microscopy (STM) is added to the set-up. STM was developed by Binnig and Rohrer in 1982 and is a very well established tool for characterization of nanostructures by imaging with nanometer resolution. The working principle is based on the quantum mechanical tunneling effect. A small potential barrier enables electrons to pass through the classically forbidden zone of the tunneling gap and to remerge on the other side. The tunneling current is created between the apex of the metal tip and a smooth conductive metal substrate. The gap distance is very important. If the gap is too big the tunneling current cannot be provided. Normally, the gap distance between the tip and the sample is approximately one nanometer. The tunneling current is also used as feedback loop to keep the position of the tip along the Z-direction with the help of piezo elements. Also the lateral movement (XY) is controlled with piezo elements.

Figure 2-7 shows a schematic of the used Raman set-up and the work principle will be explained in this section. The Raman set-up is placed on an optical table to avoid vibrations. In addition, the set-up is designed with a 50X long working-distance (10.6 mm) objective that leads to a high photon density in the focus of the monochromatic laser light. Further, the emitted back scattered light is collected along the same path as the incident laser light. The back-scattered geometry enables an improved Raman intensity through collection of the overall scattered photons with an objective that has a high numerical aperture of 0.5. The stage is adjustable in the XY-direction (motorized) and the objective in the Z-direction (piezo stage). The moving allows us to find the laser focus and to move the sample through the laser focus. The monochromator in the spectrograph (Horiba iHR 550) divide the signal in the spectral parts and is analyzed on the CCD chip of the nitrogen-cooled CCD camera. An ultra-step long-pass edge filter (Semrock RazorEdge LP02-633RE-25) and the dichroic long-pass beam splitter (Semrock RazorEdge Dichroic LPD02-633RU-25) are used to filter the laser line and to cut of the stray light. The linearly polarized λ_{ex}= 632.8 nm He-Ne laser (REO LSRP-3501, 35 mW maximum) is designed in side-illumination with an angle of 55° between the objective and the sample. The STM (Keysight Technologies GmbH 5420) is mounted on a piezo stage. With the help of the white light source, the control through the CMOS camera, the objective, the independently movement of tip and objective is it possible to focus the laser beam with a spot size of 0.5 µm tightly on the apex of the gold tip with a diameter around 20 to 50 nm.

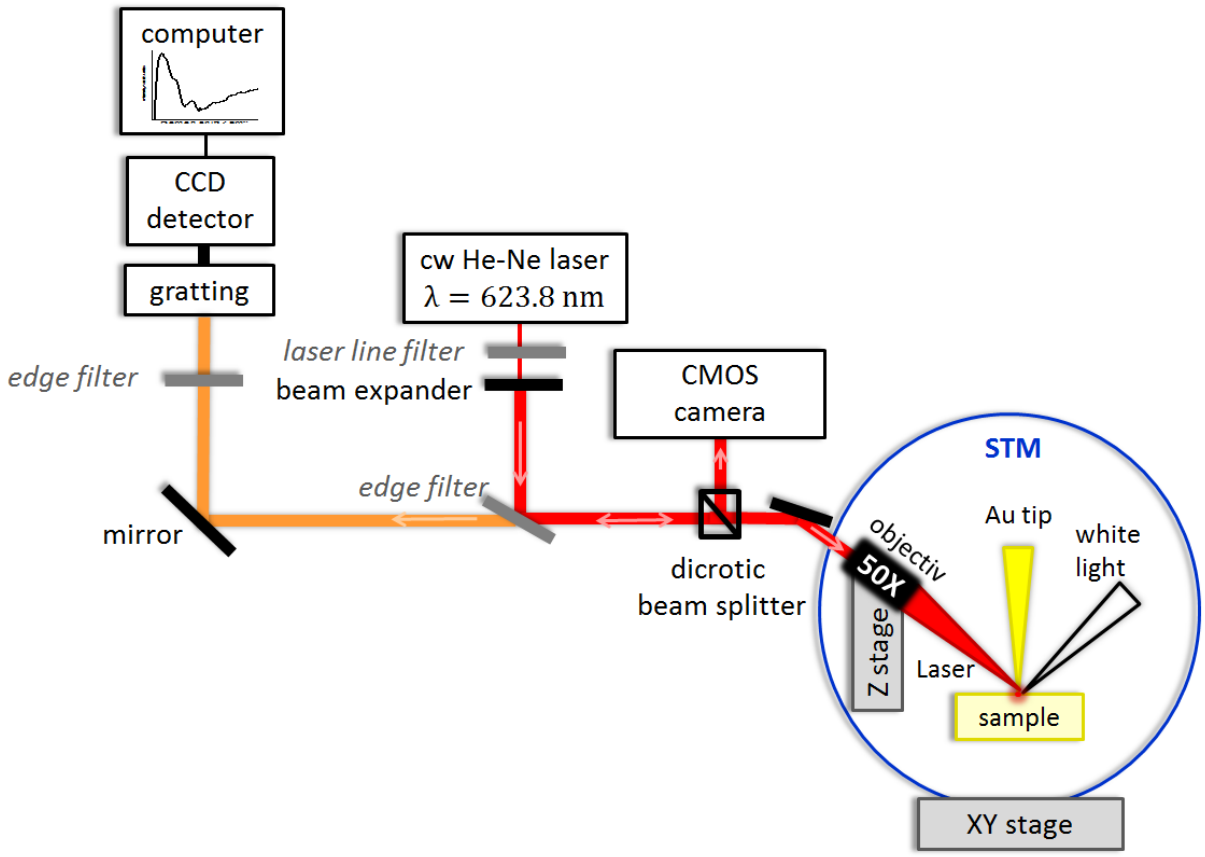

Figure 2-7: Schematic of the Raman set-up with the laser beam path. The He-Ne laser is focusing on the long-distance working objective on the sample. The back-scattered light is collected with the same long-distance working objective and is pass through a series of filter and optics to the CCD detector.

The set-up enables the detection of very low numbers of adsorbed molecules. The set-up is used for two enhanced Raman techniques; TERS needed the STM and a flat metal substrate. The other technique is SERS, which does not need the STM but depends on a rough metal substrate. With both powerful techniques an adsorbed monolayer can be investigated. For example, the degradation behavior of an adsorbed monolayer on a metal surface can be investigated. In the following chapter quantum dots (QDs) are introduced, especially lead sulfide (PbS) QDs. Since this material has promising properties for photovoltaic applications and is therefore analyzed in this thesis.

2.6 Properties of PbS QDs

Quantum dots are particles in the size of nanometers. By such orders of magnitude, the material properties become a function of the particle size and differ strongly from material properties of the bulk material. The unique properties of semiconductor quantum dots results from the phenomena of "*quantum confinement effect"* (QCE).[48] The QCE describes the dependency of the emitted wavelength from the size of the QD. The smaller the particle size the stronger is the confinement.[48,49] Semiconductors are special materials due to their bandgap. The bandgap makes it possible to change the electrical and optical properties after the absorption a photon of a semiconductor like lead sulfide. After the absorption the electron is lifted from the valence band in the conduction band.[48,50] The electron leaves in the valence band a positive charge, known as hole and create in the conduction band a negative charge. This electron-hole pair is called exciton and both charges are attracted to each other by the electrostatic Coulomb force. The Bohr radius, describes the distance of the charges. The exciton is described with the same equations as the hydrogen atom, due to the interaction of charges are quite similar. QDs are smaller than the Bohr radius of a material.

Therefore, a QD is confined in all three dimensions and is comparable with the system *"particle in a box"*.[49] Thus, it is not possible to separate the positive and the negative charge in a larger radius as the size of the QD. After the law of quantum mechanics, the distance of the charges should be equal to the Bohr radius. The charges are closer together as it is postulated by the laws of quantum mechanics. Therefore, a higher amount of energy is necessary to create an exciton. The reduction of the particle size of a QD leads to an increase of the bandgap due to the higher energy, which is needed to approach both charges. In comparison to the bulk materials adsorbs and emits a QD light with smaller wavelengths (higher energy). This means QDs experience a blue shift with decreasing particle size. The bandgap energy of a nanoparticle is the summation of the exciton energy and the bandgap energy of the bulk material.[2]

Lead sulfide quantum dots are highly interesting for scientific research and technological applications as small bandgap semiconductors. PbS QDs have a promising future for optoelectronic and photovoltaic devices like sensors, solar

absorbers and light emitting diodes. This section shows a briefly overview of the properties of PbS QDs. It is possible to engineer band gaps for PbS from bulk material with 0.41 eV to 1.8 eV for QDs by tailoring the QD size. The PbS exciton Bohr-radius is relatively large with 20 nm, this allows strong confinement effects also in larger particles, which are easy to produce and give better tolerances in size distribution. For PbS QDs the effective masses and mobility for hole and electron are similar, thus enable a simultaneous transport of both and make it to an ambipolar material.[7,51] Additionally, the Bohr radius of holes and electrons are inversely proportional to their effective masses. Thus, it is possible to confine both, hole and electron, in the same manner to discrete energies. Also, the large surface to volume ratio is a big difference in comparison to bulk material, which enables new applications. PbS QDs have a centrosymmetric rock-salt crystal structure with the space group Fm3m (No. 225) and a lattice parameter of 5.934.[52] Unfortunately, PbS QDs has an affinity to oxygen and humidity which results in a fast degradation. This problem is explained in the next section.

2.6.1 Degradation of PbS QDs

PbS QDs are more stable than dye and some other QDs. Nevertheless, they are quite sensitive to oxygen (O_2) and humidity (H_2O) and an intensive study of PbS QDs is necessary. The degradation process is not fully understood in detail.[16] Within minutes they are prone to oxidation by absorption of O_2 and H_2O, which change their properties drastically. In one week photovoltaic devices based on PbS QDs suffer from degradation around 85% of their original efficiency is lost. The challenge is to overcome the poor stability of PbS QDs under ambient conditions. Until now, PbS-QDs photovoltaic devices require a production under inert conditions to reach “high” efficiency. One application in the future shall be the fabrication of high-performance air-stable quantum dot sensitized solar cells (QDSSC´s) that are producible with easy solution processes. For comparison of the data from degraded PbS-QDs it is important to know the particle size and the synthesis route of PbS, because of the size of PbS QDs has an influence on the Raman spectrum.[24] Therefore the used route for the synthesis of PbS QDs is described in the following section.

2.7 SILAR process

An easy, inexpensive and convenient way to generate PbS QDs at room temperature is the self-assembled method -"successive ionic layer adsorption and reaction" (SILAR), based on epitaxial growth, first reported by Ristov et al. in 1985.[53] The method is chosen for this thesis due to the high surface coverage of QDs on substrates by an in situ process that makes it very useful for the QDSSCs application and also easy is the tailoring of the particle size. During this synthesis the quantum dots are deposit directly as a thin film. The resulting product of the synthesis has to be less soluble in the solvent as the educts, otherwise the synthesis does not work. SILAR can tune the QD size by the number of adsorption cycles or by control of growing time control. The experimental procedure of one SILAR cycle to form a compound of AB is given in Figure 2-8 and is explained in the next section.

Two precursors A^+ and B^- are separately dissolved in vessels at room temperature and afterwards the QDs were produced in a dipping process cycle. At the beginning of the cycle, the substrate is immersed in the cation (A^+) solution (1) and the cations will be adsorbing at the substrate surface to form an ionic layer on top of it. Then the substrate is dipped into clean solvent (2) to rinse off the cations that are not strongly bound to the substrate. Followed by a second immersion step (3) of the substrate into the anionic (B^-) solution the ions adsorb immediately to the A^+ rich surface and forming the compound AB. Finally, the anions that are not strongly bound are rinsed away by a further dipping process (4) into clean solvent.[55] More cycles or longer growing time results in a thicker film. Further variations can be achieved by finishing with a half circle or by changing the precursor order. The characterization of that QD sub-monolayer resulting from the SILAR process was performed with enhanced methods of the Raman technique the results of this experimental research are discussed in the next chapter.

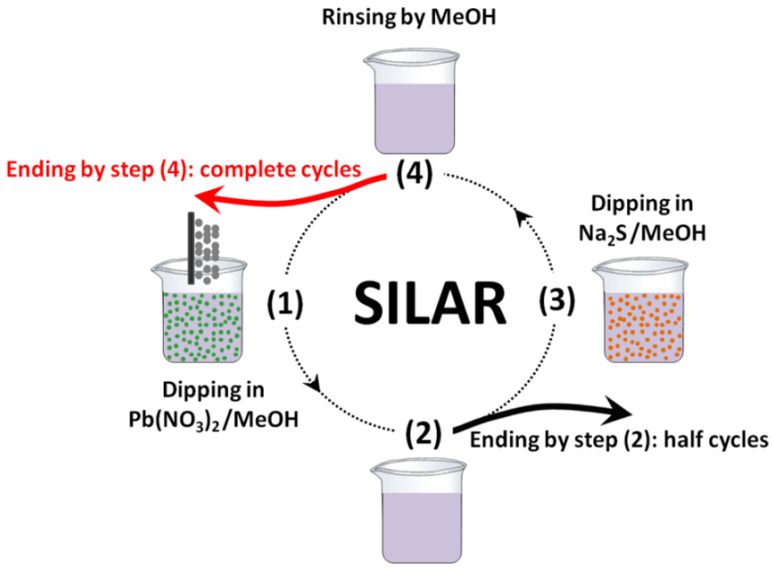

Figure 2-8: Schematic of the quantum dot nucleation process by SILAR. Hereby, cationic and anionic precursors are in separate vessels. The process can end with a fully performed cycle or with a half circle to influence the stoichiometry.[54]

3 Methods

3.1 Cleaning process

The glassware to synthesis PbS QDs was cleaned overnight in a vessel which was filled with piranha solution of H_2SO_4 (95%, Fisher Chemicals) and H_2O_2 (35%, Roth) in the ratio 3:1. The next day the glassware was subsequently extensive rinsed in ultrapure Millipore-Q water and was boiled afterwards. The rinsing and boiling process was repeated 3 further times.

3.2 PbS QDs synthesis

250 ml methanol (MeOH, HPLC-isocratic grade, 0.01% water, VWR chemicals) which was used to prepare the solutions for the PbS QDs synthesis was degassed with Ar (5N, Westfalen) for 15 min. Then the degassed solvent MeOH and the powders lead nitrate ($Pb(NO_3)_2$ (Sigma-Aldrich, 99.99%, Cas Number:10099-74-8)) and anhydrous lead sulfide (Na_2S (Sigma Aldrich, CAS Number: 1313-82- 2)) were transferred in the glovebox (MECAPLEX, Mecabox 82-1 LF) under N_2 atmosphere. In the glovebox was an atmosphere with an O_2-level between 0.5 and 4 ppm and humidity at 0.011 ppm. PbS QDs were synthesized on commercial SERS substrates (SERStrates, *„silmeco“*) based on a silicon (Si) nanostructured substrate evaporated with gold. The SERStrate were used as received without any further cleaning. The PbS QDs synthesis was done by successive ionic layer adsorption and reaction (SILAR) according to a synthesis developed in the group of Canovas.[55] For PbS QD SILAR deposition the SERStrate was dipped sequentially in five degassed solutions prepared in five different beakers. Whereby three of those beakers include the pure degassed solvent MeOH, one of those five beakers include the degassed $Pb(NO_3)_2$ solution and one beaker include the Na_2S solution. Following the SILAR process is described: The SERStrate is dipped in (1) 0.02 M methanolic $Pb(NO_3)_2$ for 20 s, (2) in MeOH for 30 s, (3) then in 0.02 M methanolic Na_2S for 20 s, (4) and in MeOH for 30 s. This cycle is known as SILAR cycle and was repeated once again. After two completed SILAR cycles on the SERStrate, the substrate with the adsorbed PbS QD was dipped in (5) MeOH for 50 s to

wash away the molecules which were not physical bound on the substrate surface. At the end the last traces of MeOH on the substrate were evaporated and then the sample was stored in a beaker wrapped with parafilm and aluminum foil. The sample was always measured that day after preparation.

3.3 Sealing process

The samples were sealed directly after the PbS QD deposition on the SERStrate in the glove box at an O_2-level between 0.5 and 2.5 ppm. For the sealing procedure, a stack of six layers parafilm (Bemis) was prepared with a 7 x 7 mm^2 cut-off square. This stack was placed on a microscope glass slide (Thermo Scientific, Menzel Glaser, 76 x 26 mm^2). The parafilm on the slide was heated to approximately 55 °C to melt the parafilm slightly. After a slightly melting of the parafilm with a hot plate the slide was removed from the hot plate. Then the sample was put into the cut off section and a coverslip (diameter of 12 mm, thickness 0.170 ± 0.005 mm, Carl Roth) was placed on top of the parafilm stack to seal the sample. Afterwards another heating step at 50 °C follow to stuck the coverslip on the parafilm. At the end, a last single layer of parafilm with a square central cut off 6 x 6 mm^2 was placed over the coverslip to close all vents on the edges between the cover slip and the stack of parafilm. All samples (sealed or unsealed) were stored overnight in the glove box and were measured the next day.

3.4 Surface-enhanced Raman spectroscopy measurement

The Raman system consists of a red HeNe laser (λ_{ex}= 632.8 nm; REO LSRP-3501, 35 mW maximum output power, linearly polarized) in back-scattering configuration, mounted on an optical table with active vibration isolation. A Horiba iHR 550 spectrograph (600 gr/mm grating, 1 cm^{-1} spectral resolution) with a CCD camera (Syncerity CCD, Horiba) is used as a detector. An Olympus 50X long working-distance objective (WD = 10.6 mm, NA = 0.5) is used to focus the laser beam onto the sample and to collect the back-scattered light. A long-pass filter (Semrock RazorEdge ultra steep long-pass edge filter LP02-633RE-25) and a dichroic long-pass beam splitter (Semrock RazorEdge Dichroic LPD02-633RU-25) with cut-off values of 79 cm^{-1} and 156 cm^{-1}, respectively, in the detection path filter out the Rayleigh elastic scattering and

address the inelastic Raman signal to the entrance of the spectrograph. The laser power is controlled with a motorized gray filter wheel (FW212C, Thorlabs) equipped with nine different neutral-density filters with optical densities ranging between 0 and 1.3. The sample was fixed with a double-sided tape onto a sample holder to measure the sample in 0°. The spectrometer is calibrated every day with a Si wafer.

For one type of sample, powers were measured subsequently at the same spot with 10 s spectral integration time at each power. The displayed power spectra are averages over 3 to 4 spots on one sample type A, three samples type B and 4 samples type C. All other measurement conditions are described in the main text of the experimental part. The background was manually subtracted with the software Igor Pro 6.34A wavemetrics, which is also described in the main text in the experimental part.

3.5 Preparation of smooth gold substrates for TERS

For TERS measurements smooth gold substrates are needed. The smooth gold film was evaporated on a 1 mm thick glass substrate (mica) by a rate of 2.5-3 Å/s until the gold layer reached a thickness of 150 nm. For the evaporation process the Edward auto 306 cryo oven was used. For the annealing process the gold on mica (Au/mica) substrate was placed in a glass petri dish and was heated in the oven for 2 hours at 500°C.

3.6 Electrochemical tip etching

Gold (Au) wires were sharpened by electrochemical etching. For the gold tip preparation, a voltage of 2.4 V is applied between the gold wire and a gold ring electrode that surrounds the gold wire. The gold wire with a diameter of 0.25 mm (5N purity, Mateck) was cut by a length of 1.5 cm and was straightened with a teflonband covered tweezer. The gold wire was cleaned with ultrapure ethanol (EtOH) by rinsing. Subsequently, after the rinsing a short and carefully flame annealing process followed. The electrochemical tip etching step follows immediately in an etchant solution of EtOH and hydrogen peroxide in the ratio 1:1. The gold wire was fixed on one end in a metal clamp and was immersed 3 mm inside the etchant solution with the other end. The gold ring around the gold wire was placed on the surface of the etchant solution that ¾

height of the gold ring was immersed in the solution. The gold wire was placed in the center of the gold ring. A large surface tension is formed between the ring and the gold wire due to the applying voltage. As a result of the process a meniscus is created within this region the etching proceeds more quickly which leads to dissolving of gold. The etching process enables the shaping of the wire in a pencil-shape apex. Finally, the rinsing with Millipore-Q water removed the rest of the etching solution from the gold tip. Whereby, the water jet for the rinsing was focused directed on the middle of the wire and not direct on the end of the tip, to avoid a bending of the apex of the gold tip due to the gold is easy deformable after the etching process. The electrochemical etched Au tip was used as STM tip.

3.7 Tip-enhanced Raman spectroscopy measurement

The TER measurements were recorded with the same Raman setup as described in the previous section 3.4. The detector was changed to Horiba iHR 550 spectrograph (600 gr/mm grating, 1.65 cm^{-1} spectral resolution), nitrogen-cooled CCD camera (Symphony II, Horiba). The laser was focused to the tip by a piezo controlled stage. To simplify the focusing of the laser spot to the apex of the gold tip a white-light fiber (KL 1600 LED, Schott) and a CMOS camera (MC 1362, Mikrotron) were used. As explained in the section 2.4 is the STM needed for TER measurements to approach and retract the gold tip from the sample. The STM was mounted onto a x,y piezo stage (custom-made by Steinmeyer Mechatronics, former Feinmess Dresden). The used parameters are listed in the main text in the experimental part.

3.8 Atomic force microscopy

For atomic force microscopy (AFM), a dimension icon with ScanAsyst was operated in tapping mode. OTESA Cantilevers from Brucker were used in resonant frequency of 300 kHz. Areas of 1 µm by 1 µm and 5 µm by 5µm were scanned with a resolution of 512 pixels by 512 pixels (appendix Figure 6-3). Further the PbS QDs on gold were measured with an Agilent 5500 STM (Company Keysight). The used parameters are listed in the main text in the experimental part.

3.9 Scanning tunneling microscopy and energy dispersive X-ray spectroscopy

The scanning tunneling microscopy (STM) measurements were collected from an Agilent 5500 STM (Company Keysight).

3.10 Scanning electron microscopy

The nanostructure of the PbS QDs, were characterized by scanning electron microscopy (SEM) with a Hitachi SU8000. Also the PbS QDs were investigated with the energy dispersive X-ray spectroscopy (EDX). The etched gold tips were characterized by a Zeiss 1530 Gemini Leo. The tips and the substrates with PbS QDs on top were placed on 8 mm diameter aluminium stubs. The used parameters are listed in the main text in the experimental part.

4 Experimental results

In this thesis three PbS QDs samples with different oxygen contents were analyzed to study the influence of oxygen on the degradation behavior. Sample A was a sealed sample where the PbS QDs were *"catched"* in a nitrogen environment. Sample B was also sealed but during the synthesis and the preparation of the sample the oxygen content was higher than in sample A. That means sample A and B were measured in a nitrogen atmosphere with different contents of oxygen. Sample C was also prepared in the glovebox but without a sealing, that means the sample was measured at ambient conditions including oxygen and humidity, both leads to oxidation.

In the next chapters the SERS substrates were characterized with scanning electron microscopy (SEM). Also, the sealing procedure is explained and the characterization of the prominent peaks which were measured with SERS. Additionally, calculations were done to determine the quality of the SERS reproducibility and the comparison of two different SERS substrates was done.

4.1 Characterization of SERS substrate

As known from section 2.3.2 the geometry of SERS substrates influences the enhancement of the Raman signal, which depends on the quality of "*hot spots*" formation. A good SERS substrate creates a lot of homogeneous and stable "*hot spots*" on the surface area and enables an easy sample deposition on the substrate.

4.1.1 Comparison of SERS substrates

Depending on the manufacturing and/or the creation of "*hot spots*" some SERS substrates contain fewer variations than other substrates. Figure 4-1A compares the PbS QDs absorbed on two different structured SERS substrates. Each spectrum is an average of 12 spectra, measured with a laser power at 0.89 mW and an integration time of 10 s. The SERS substrate from the company *"Clarite"* (Figure 4-1B) is based on the structure of inverse gold pyramids. This allows a stable structure of the substrate even during and after the sample preparation in a wet solvent process. Due to the stable and homogeneous structure of the inverse pyramids a strong enhanced SERS signal is

obtained with less area dependency. The QDs have a stronger enhancement closer to the tip of the inverse pyramid.

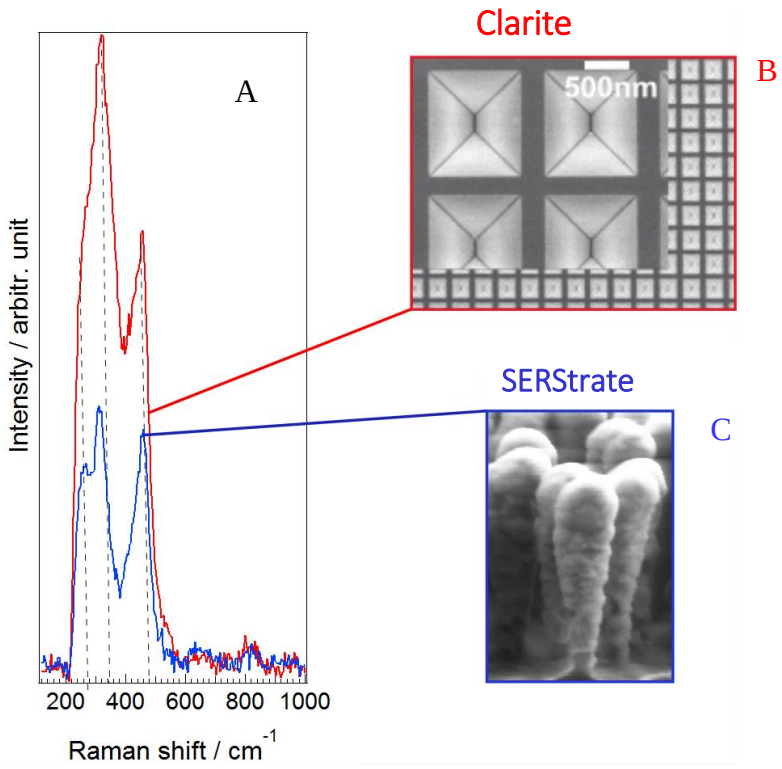

Figure 4-1: A) Comparison between the SERS signal intensity of PbS QDs on different structured substrates. B) The *"Clarite"* substrate involves inverse gold pyramids and the C) *"Silmeco"* substrate involves nanopillars. The PbS QDs were excited with λ_{ex}= 632.8 nm and an integration time of 10 s. The Raman intensity in the *"Clarite"* substrate has nearly double the high as the *"Silmeco"* substrate. Also it is visible that the positions of PbS QDs peaks in the *"Clarite"* substrate are shifted in comparison with the *"Silmeco"* substrate. In the first mean peak the signal is 40 cm^{-1} shifted and in the second main peak the Raman signal is 35 cm^{-1} shifted. Also in the *"Silmeco"* substrate a clear shoulder like peak around 278 cm^{-1} was detected in comparison to the *"Clarite"*substrate which has a very less signal at 278 cm^{-1}.

The SERS substrate (SERStrate, Figure 4-1C) from the company *"Silmeco"* is based on gold nanopillars. The SERStrate was used to generate "*hot spots*" after the solvent evaporation. The change from the SERS substrate by the company *"Clarite"* to the SERStrate by the company *"Silmeco"* occur due to the fact that *"Clarite"* were no longer available on the market. The QDs were produced with a non-degassed solvent which also included some traces of water and were measured with the Nikon Eclipse Ci Raman microscope. The difference was calculated between the relative intensities of the

two most prominent peaks (Figure 4-1A). The two main bands of the QDs were at 336 cm^{-1} and 485 cm^{-1} for the "*Clarite"* SERS substrate and at 320 cm^{-1} and 475 cm^{-1} for the *"Silmeco"* SERStrate respectively. The two different nanostructured SERS substrates shows a variation, around 13.6% (appendix 10.1, Figure 10-1). The stronger enhancement for the *"Clarite"* SERS substrates could follow due to the fact that most of the adsorbed QDs were close to the tip of the inverse pyramid. That could be caused by the fact of solvent evaporation process, which results in a strong and stable enhancement. The less intense signal of the SERStrate could be based on the non-homogenous quality of "*hot spots*". Due to the quality distribution of "*hot spots*" multiple areas were analyzed in order to compensate the discrepancies and to get reproducible information as it is explained in the next section.

4.1.2 Analysis of SERStrate

The PbS QDs were deposited on a SERStrate with silicon gold coated nanowires from the company *"Silmeco"*. The SERStrates were used as received by the manufacturer. From now on all the presented measurements were taken using those substrates and were measured on a self-made Raman setup, which was illustrated in chapter 2.5 (The same Raman setup was also used for the TERS measurements). A two weeks old sample with PbS QDs, stored in the glovebox under nitrogen conditions and characterized with SERS technique, was also probed with SEM to analyze the substrate structure of the silicon gold coated nanowires. Figure 4-2A shows a 5 micron zoom out area of the nanopillar structure and indicates homogenous self-assembled parts of *"hot spots"* over the whole sample surface. The solvent evaporation on the substrate after the SILAR process leads to surface tension, which forced the nanopillars to lean towards the nearest neighbors. The zoom in at 2 micron, in Figure 4-2B indicates different group sizes from two to six leaned nanopillars and some single standing nanopillars. The use of a further zoom in at 500 nm (Figure 4-2C) shows an additional variation factor. The lean on effect of the pillars varies strongly from group to group and even within a group the creation of *"hot spots"* was non-uniform. Consequently, the enhancement of the obtained SERS signal is expected to suffer from moderately inhomogeneous SERStrates before and after QD sensitization. Additionally, variations can also be expected from substrate to substrate. Therefore, the relative intensities

between the most prominent peaks in three different spots were calculated for the three samples A, B and C. The values obtained for the spot-to-spot variation are 2.56% (sample A), 3.40% (sample B) and 0.79% (sample C) (appendix, Figure 6-1). All samples show spot-to-spot reproducibility of relative peak intensities.

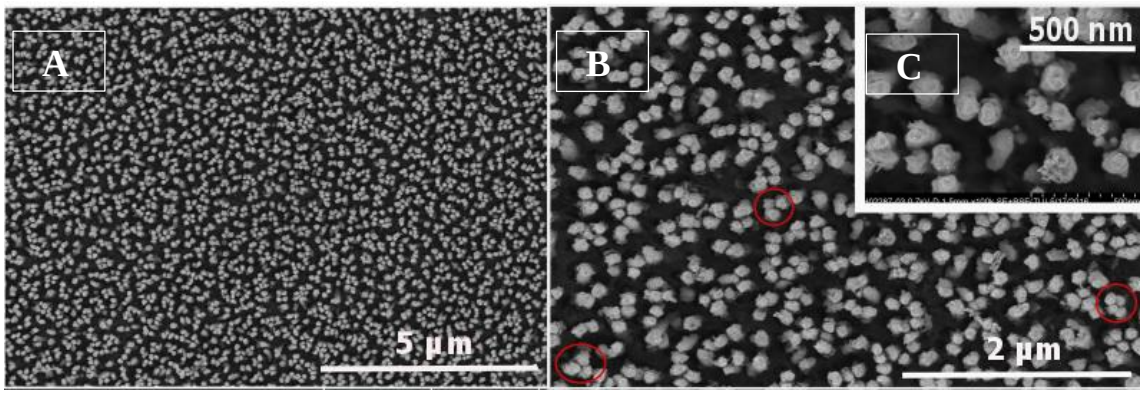

Figure 4-2: A) Silicon gold coated substrate with nanopillars create *"hot spot"* areas due to surface tension. The zoom out area with a scale bar of 5 micron shows a various creation of "*hot spot*" areas. B) The zoom in area, with a scale bar at 2 micron indicated the inhomogeneous within the invested area due to a different group size of nanopillars and a different strong lean on effect between the pillars within the group, three of those examples are marked with red cycles. C) A further zoom in with a scale bar at 500 nm clearly illustrates the different "lean on" possibilities in the sample.

Based on Figure 4-2 there are areas where the signal will be increased due to *"hot spot"* areas. The calculation determines spot-to-spot variation in terms of absolute and relative intensities between main bands. However, the numbers obtained are not small enough to overcome the effect by means of statistical treatment. Thus, for the data analysis, several spots were measured at each sample and several samples of the same type have been analyzed. The results were averaged to minimize spot-to-spot variation and substrate-to-substrate variations.

4.1.3 PbS QD distribution on SERStrate

Another influence on the enhancement factor is the distribution of the PbS QDs on the nanopillars. The sample from Figure 4-2 was investigated to analyze the PbS QDs deposition on the SERStrate. Figure 4-3A shows the adsorbed PbS QDs on nanopillars and indicate a low and inhomogeneous coverage of isolated PbS. As explained in chapter 3 the strongest "*hot spots*" are created between post-leaned pillars

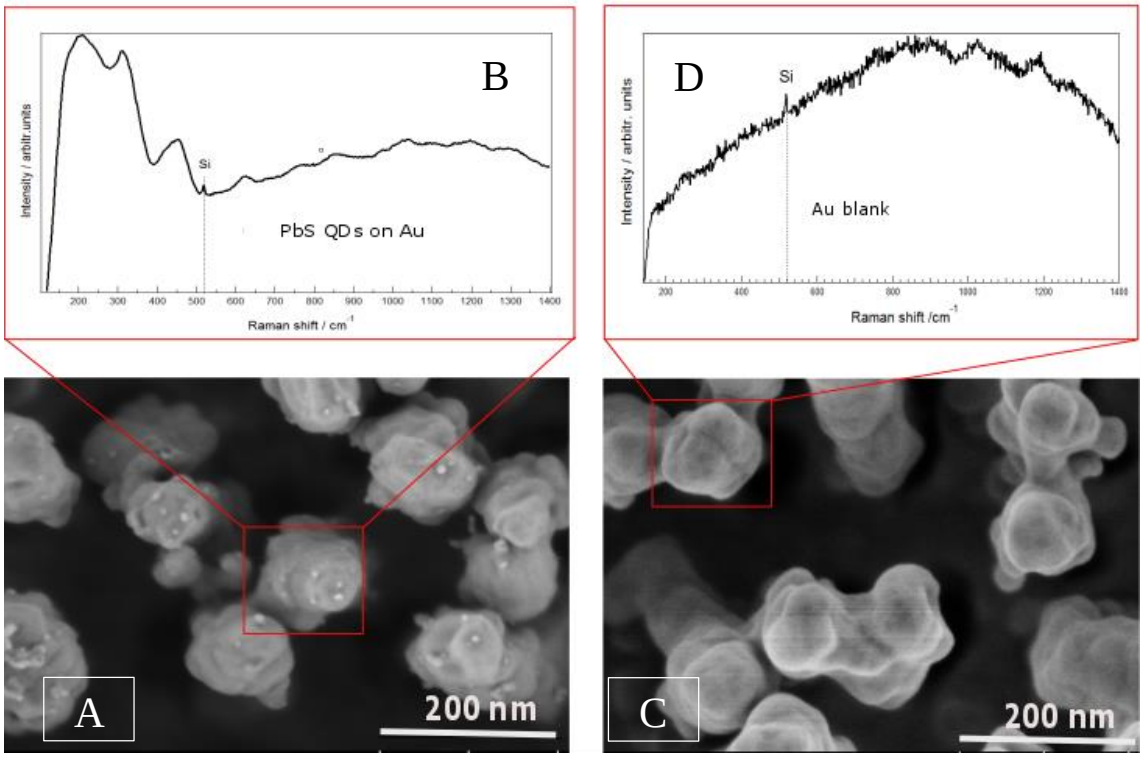

Figure 4-3: A) PbS- QDs on silicon gold coated SERStrate, with a zoom in with a scale bar of 200 nm. The spectrum B) of the sample clearly showed the QD vibrational fingerprint. C) Reference image of the silicon gold coated SERStrate (blank) stored under the same conditions as the sample, also with a scale bar of 200 nm. The spectrum D) of the reference sample showed the gold signal with the silicon peak.

Figure 4-3B illustrates SER spectra of PbS QDs on a SERStrate under ambient conditions detected without impurities. The 8 to15 nm dots are identified as PbS QDs. In Figure 4-3C the reference of the SERStrate is shown. The reference was stored under the same conditions as the sample in Figure 4-3A, and showed no impurities on the surface Figure 4-3C.

Figure 4-3D shows the SER reference spectrum of a SERStrate with a pure gold background and the silica peak under ambient conditions without impurities and PbS QDs signals.

For a further characterization of the existence of PbS QDs, EDX was performed on a flat substrate of Au/mica following the same technique as for the deposition at PbS QDs on gold coated SERStrates. The measurement detected a presence of lead and sulfide and is shown in the appendix (Figure 6-2 and Figure 6-3).

Also, AFM measurement of the PbS QD sample of the SERStrate in Figure 4-3A was performed, which indicate the structure on the pillar surface. In the "*phase mode"* an additional structure was detected, which could belong to the PbS QDs (appendix, Figure **6-4**)

4.1.4 Determination of measurement variations

This chapter shows the reproducibility of the measured samples. The spot to spot variation was calculated in the samples A, B and C. Also, the fluctuation within one spot in the samples A, B and C were calculated.

As previously discussed, depends the variation on substrate manufacturing and influences strongly the enhancement from spot-to-spot and from substrate to substrate. Furthermore, there is a loss of SERS activity because of the laser power that changes the gold surface of the nanopillars.

To determine if and how strong the substrate variation influenced the obtained spectra, the spot-to-spot variation was calculated from three different spots from each sample A, B and C (appendix, Figure 6-1). Therefore, the samples A, B and C were exposed to a low laser power at 0.15 mW with a focused spot size of 500 nm in diameter and a calculated power density of 1.8×10^9 W/m^2. The spots were recorded with an integration time of 10 s. The relative intensities of the most prominent peaks at 192 cm^{-1} and 312 cm^{-1} indicated a difference in the spot-to-spot variation of 2.5% for sample A, 3.4% for sample B and 0.79% for sample C.

The idea to measure the SER spectra for a certain time at low laser power had the aim to verify if the vibrational fingerprint of the recorded spectra of PbS QDs was influenced by the excitation beam and to find out the signal-to-noise for the spectra. When the spectra do not change, we can confirm that the illumination over a short time at low laser power does not have an influence on the chemical state. Therefore, three different spots (laser parameter were the same as in the spot-to-spot calculation) of the samples A, B and C were recorded with an exposure time (10 s integration time for each spectra). Figure 4-4 presents one of those measured spots for each sample. The different colored line in each spectrum in Figure 4-4 illustrates a single spectrum of those measured spectra for each sample, which were measured on one focused spot. The

signal fluctuation was calculated between the background and the maximal intensity at background corrected spectra to ± 9% for A (15 spectra), ± 13% for B (7 spectra) and ± 10% for sample C (11 spectra). Figure 4-4 shows no changes during the excitation time. The relative band intensities seemed to be unchanged. Therefore, it can be expected that the illumination at low-power do not caused degradation artifacts.

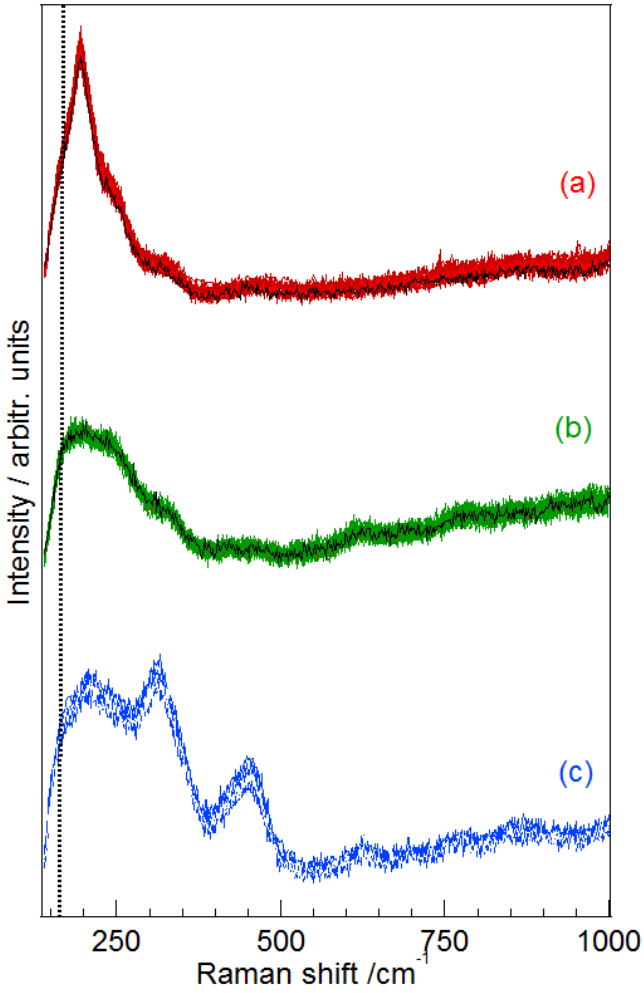

Figure 4-4: Time series for PbS /Au for sample A (a), sample B (b) and C (c) for 30 spectra at the same sample spot for 300 s (10 s integration time with 0.15 mW). A single spectrum of every time series is highlighted. The dotted line indicates the dichroic-filter cut off at 156 cm $^{-1}$.

The obtained spot-to-spot variations are small for relative peak intensities, same as the variation of the fluctuation. The summarization of different spots within one SERS sample leads to reproducible relative peak intensities during the SERS measurement.

The Raman signal is sensitive to environmental conditions and can be changed with the laser wavelength. Therefore, sample A and C were also measured with an excitation beam of λ_{ex}= 785 nm (appendix 6.4, Figure 6-5) and presented the same trend as with the center wavelength of λ_{ex}= 632.8 nm excitation. Thus, it can be assumed that the Raman signal was not influenced by energy and the changes were caused only by oxygen.

4.2 Difficulties at the PbS QDs sealing

For the study of PbS QDs it was necessary to *"cage"* the sample in an inert atmosphere (O_2-level 0.5-4 ppm, humidity 0.011 ppm). The sealing is a possibility to produce such an inert environment for the sample. The sealing method is explained in detail in section 3.3. Figure 4-5 shows the schematic of a sealed sample, whereby the microscopic glass slide (purple area) was the basis. A cut-off square of parafilm (dark grey area) was placed on the glass slide and the SERStrate with the PbS QDs submonoayer (orange square) was placed in the cut-off area of the parafilm square. Finally, a glass cover slip (bright grey area) was put on top of the parafilm stack and a last single layer of parafilm with a cut-off square was put on top to complete the sealing and avoid any vents.

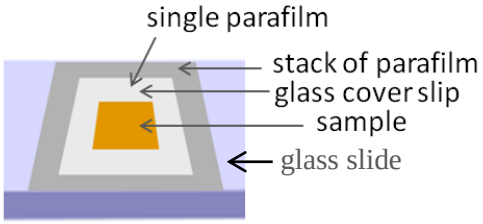

Figure 4-5: The sealing process *"catched"* the sample in an inert volume with less content of oxygen and humidity to avoid oxidation. A stack of parafilm with a cut off square is placed on a glass slide. The SERStrate with the PbS QDs on the surface is placed in the middle of the cut-off square and covered with a cover glass slip. Finally, a last layer of parafilm also with a cut-off square is placed over the cover glass slip to avoid vents.

During the preparation of the sealed samples in the glovebox trace amounts of oxygen can alter the chemical state of PbS QDs. Furthermore, no differences of badly covered parts or holes in the heated parafilm were observable. But it is conceivable that the

parafilm was not closely attached on all parts at the interface between the glass slide and the parafilm after the heating process. Those vents were not detectable by eye. Improvements are necessary and will be discussed in detail in chapter 4.5.2.

4.3 Raman background subtraction

To compare the relative intensities of SER spectra it was necessary to subtract the background. Initially, it was tried to remove the background with a fit function in the technical and data analysis program *"Igor Pro 6.34A"* from *wavemetrics* but it was not possible to fit the background shape with a mathematical function. Therefore, the background was removed from the spectrum by hand. Thus "LabSpec5" from the company *Horiba* was used to remove the background. The spectrum was loaded in the program and by using the function *"add baseline points",* it was possible to mark the background manually with single points (Figure 4-6A).

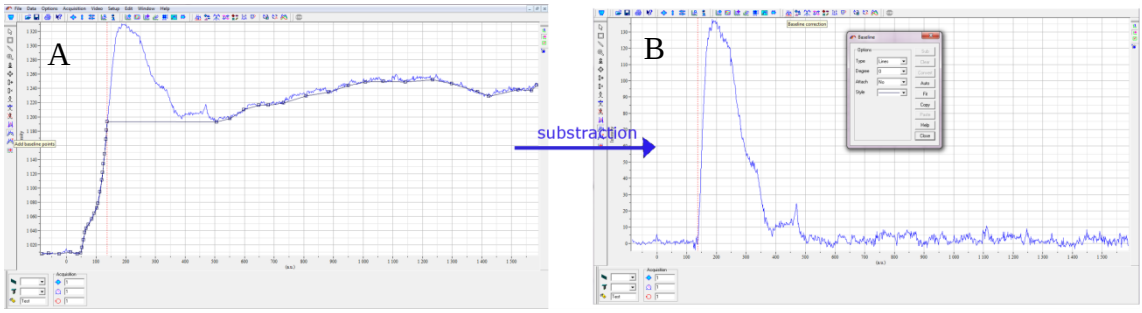

Figure 4-6: Background of SER spectra were manual marked (A) and subtracted (B) with a function in *"LabSpec"*.

This background subtraction required an accuracy that the points were set on the same position on each spectrum for one sample. Otherwise it would influence the resulting spectrum and could lead to changes on the relative peak intensities. With the functions *"baseline correction"* (Figure 4-6A) and *"subtraction"* (Figure 4-6B) was it possible to subtracted the background.

4.4 Characterization of PbS QDs degradation

The aim for that study was to understand the influence of the oxygen content and photothermal effect of the oxidation process of PbS QDs which are prone to oxygen.

Therefore, three different samples of PbS QDs on gold were used with different oxygen levels. The samples were analyzed with a λ_{ex}= 632.8 nm He-Ne laser, which is in resonance with the plasmonic field of the gold substrates. All three samples were synthesized (chapter 3.3) under the same conditions and same parameters in a glovebox under nitrogen that included less than 0.011 ppm humidity and an oxygen content between 0.5 and 4 ppm. Two of those three samples were sealed directly after the PbS QD synthesis. The sealing should avoid degradation from oxygen. The third sample did not get any sealing. It was used as it was obtained after the PbS QDs synthesis.

The obtained results of the vibrational signature of PbS QD degradation are published in the journal "Vibrational Spectroscopy" under the title "The SERS signature of PbS quantum dot oxidation". The figures from the sections 4.1.4, 4.4.1 and 4.4.2 used in this thesis are a modified version of the graph in the mentioned manuscript. Also the discussion from the sections 4.1.4, 4.4.1 and 4.4.2 is based on the discussion of the paper.

4.4.1 Influence of the ambient conditions

The samples were produced on four different days. One sealed sample and one oxygen sample were always generated on the same day. In total four sealed and four oxygen samples were obtained. One of the four sealed samples showed a different behavior in comparison to the other three sealed samples. The sealed sample that looks different from the other three is present now as sample A, the three sealed samples with the same behavior where averaged to sample B and the four oxygen samples were averaged to sample C. The samples A, B and C were measured at 0.15 mW with an integration time of 10 s. The samples were background subtracted with the program *"Igor Pro"* (waveMetrics) as explained in the section 4.3 and normalized to the intensity at 196 cm^{-1} for a better comparison. The cut-off region at 156 cm^{-1} of the dichroic filter is marked in Figure 4-7 with a grey dotted line. The sharp peak at

518 cm-1 is obtained from the silicon gold coated substrate and is characterized with an asterix (*). The background of the reference spectrum of the SERStrate (blank) was also subtracted and is shown in the Figure 4-7 illustrated with a y-offset for comparison.

Sample A (Figure 4-7a) shows a strong and sharp peak at 196 cm^{-1}. The peak is close to the dichroic filter cut-off at 156 cm^{-1} but still separated. A shoulder peak came up at 235 cm^{-1} and a shoulder-like peak was detected at 312 cm^{-1}. Those three peaks overlap with each other. A broad band around 450 cm^{-1} includes two overlapped peaks which were detected at 430 cm^{-1} and 460 cm^{-1}. This consumption does not claim that those are the only peaks in the area from 150 cm^{-1} to 312 cm^{-1}. However, at the following discussion only the most prominent peaks are considered.

Sample B (Figure 4-7b) shows at the peak position 235 cm^{-1} a sharper defined peak in comparison with sample A and has nearly the same relative intensity than the peak at 196 cm^{-1}. The Pb(sulf)oxide peak at 312 cm^{-1}, 430 cm^{-1} and 460 cm^{-1} increased compared to the presented peak from sample A. As well the relative intensities of the peaks at 430 cm^{-1} and 460 cm^{-1} were increased. The peak at 614 cm^{-1} was detected the first time in sample B.

Sample C (Figure 4-7c) was measured under ambient conditions, including oxygen and environment humidity. The relative peak intensities at 235 cm^{-1} and 312 cm^{-1} increased in comparison to the relative peaks intensities of the sample A and B. The relative intensity from the peak at 312 cm^{-1} nearly came up to the relative band intensity of the detected peak at 196 cm^{-1}. The PbS LO peak appears a little blueshifted from 196 cm^{-1} to 210 cm^{-1}. Baranov et al. indicated a decreasing crystal size with a blueshift as expected in relation to the quantum confinement effect. The blueshifted peak moved closer to the 235 cm^{-1} peak that could indicate an ingrowth of Pb(sulf)oxide bands at 234 cm^{-1} and 287 cm^{-1}. Furthermore, there was an increase in relative intensities at 430 cm^{-1} and 460 cm^{-1} which is assumed from an increase of oxygen. Also, the relative peak intensity at 614 cm^{-1} was detected and increased in comparison with the relative intensity of sample B and sample A.

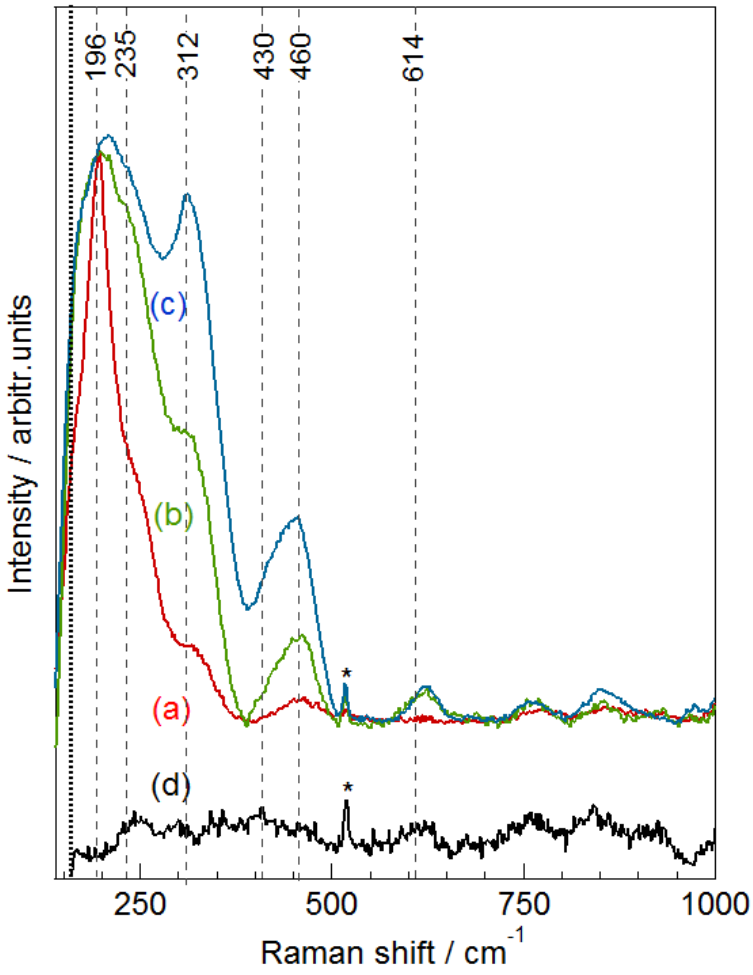

Figure 4-7: The SER spectra present three different samples of PbS QDs/Au (a-c). The samples were measured at 0.15 mW, background subtracted and normalized to the peak of 196 cm^{-1}. The blank (d) was also background subtracted with a y-offset. The dotted line marks the dichroic filter cut off at 156 cm^{-1}. The axterix (*) marked the Si needle support from the SERStrate. The Si needle support caused on the substrate manufacturing (single Si peaks are covered with gold).

For a validation of the obtained peaks of PbS QDs on gold from the samples A, B and C the literature was studied but also reference spectra of the most prominent oxidation products and from PbS bulk were taken on the same setup (ambient conditions, λ_{ex}= 632.8 nm and room temperature). Figure 4-8a shows the measurement of the reference spectrum from PbO_2 (287 cm^{-1}, 384 cm^{-1}) that was measured with 10 s spectral integration time at 0.95 mW. The reference spectrum of $PbSO_4$ (238 cm^{-1}, 614 cm^{-1}, 443 cm^{-1}, 980 cm^{-1}, Figure 4-8b) and reference spectrum of PbS (234 cm^{-1} and 460 cm^{-1}, Figure 4-8c) were measured with an integration time of 30 s, 4 accumulations

at 19.8 mW. Those reference spectra were helpful to valid the band assignment to the measured PbS QD data.

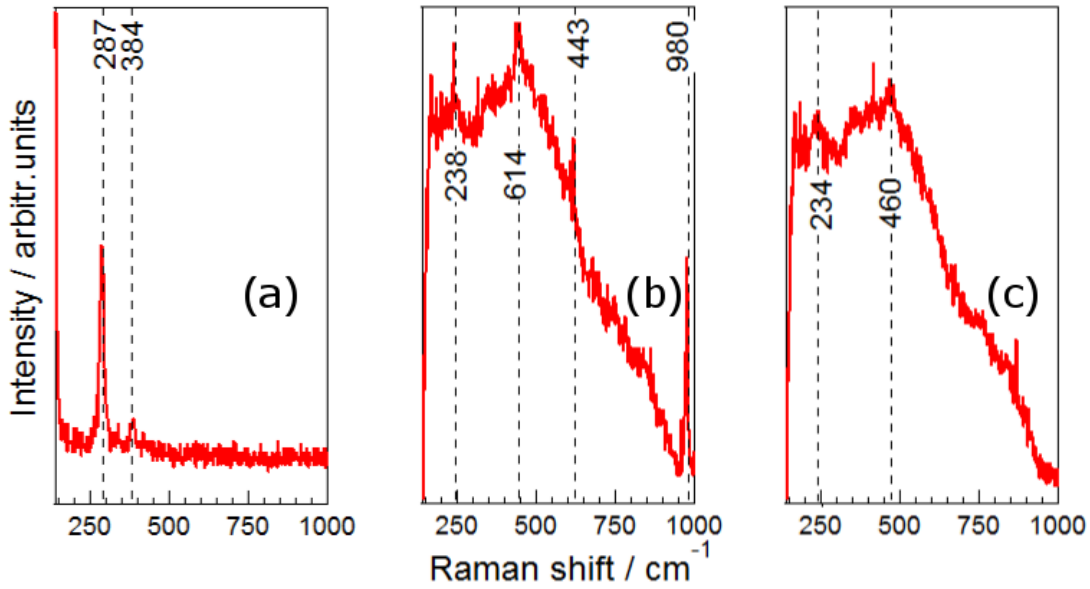

Figure 4-8: Measured reference spectra of a) PbO_2, b) $PbSO_4$ and c) PbS to compare those detected signals with the detected signals of the PbS QDs with different degradation levels.

The Raman peaks of the SER spectra at 196 cm^{-1}, 235 cm^{-1} and 450 cm^{-1} can be assigned to the phonon modes of the PbS structure.[56,57,58] Whereby the first two bands 196 cm^{-1} and 235 cm^{-1} belongs to the longitudinal optical mode (LO)[25,25] and the third band 450 cm^{-1} to its first overtone of the longitudinal optical mode (2LO).[57,58] Krauss et al. calculated the band structure to assigned the obtained PbS photons.[57,58] Moreover, the band at 450 cm^{-1} can be contributed to two-phonon scattering.[57] The peak at 312 cm^{-1} does not belong to the PbS phonon mode and can be assigned to the lead oxidation product Pb_3O_4.[59,60,61] Furthermore, Pb_3O_4 has a doublet around 450 cm^{-1} that could overlap with the first overtone of PbS.[62] A further signal from those Pb-oxide species[60] is obtained at 450 cm^{-1}. The broadening of the discussed bands may be due to the overlap of the Pb-oxide species with the 2 LO PbS mode.[62]

The sample comparison showed that sample B follows the trend of sample A but some oxidation signatures linked to sample C like the upcoming band at 612 cm^{-1} and the broadening of peak at 196 cm^{-1}. Figure 4-8b indicated the peak at 614 cm^{-1} as $PbSO_4$ species, also the literature indicate that peak as lead sulfate.[23,62] Sample A and B were

fabricated in the same way. It can be assumed that the sealing method was better for sample A than sample B. Further it can be supposed that the O_2-level in the glovebox was not stable and the higher oxygen content leads to a higher degradation behavior in sample B. Hence, the PbS LO phonon mode is less prominent compared to sample A. The relative intensities at 312 cm^{-1} and 612 cm^{-1} from sample B and C were increased. The wide band in the range of 450 cm^{-1} became broader with an increase of oxygen. The relative intensity of the PbS LO mode at 195 cm^{-1} is more intense as the PbS 2 LO mode at around 450 cm^{-1}. Thus, the increase of the relative intensity in the area 400 cm^{-1} to 500 cm^{-1} can be directly related to the oxygen amount.

Furthermore, the relative intensity of the pure oxidation peak at 312 cm^{-1} became more intense and sharp with higher content of oxygen. The stronger and sharper the peak at 312 cm^{-1} is the more crystalline is the lead oxide product. It can be assumed the formation of crystalline PbS in lead oxide products and after a higher degree of oxidation it forms stable lead oxide products that probably grows into the core of the PbS QD and results in a high and sharp detectible peak of lead oxide products at 312 cm^{-1}. The sample B gave an impression of the formation but is surely more related to the condition of sample A. The sharp and very strong peak at 196 cm^{-1} will be broader and from sample A to sample B the two PbS LO modes (196 cm^{-1} and 235 cm^{-1}) became nearly similar. The change from sample B to sample C indicated a broad band including the signal at 196 cm^{-1} and 235 cm^{-1}. The shoulder like peak at 235 cm^{-1} disappeared slowly with a higher content of oxidation product and the peak at 312 cm^{-1} began to create a sharp peak.

As a first summary is can be assumed that sample A seemed mostly intact and showed the vibrational fingerprint of non-degraded PbS QDs. The less obtained oxidation in sample A may be caused by oxygen content that was present during the QDs fabrication in the glovebox. The sharp PbS phonon mode (LO) at 196 cm^{-1} of sample A is assigned to a higher level of crystallinity and is better as for the phonon modes at 235 cm^{-1} and 450 cm^{-1}. Moreover, the crystallinity of sample A is better than in the samples B and sample C. Consequently, the spectral signature of PbS QDs for sample A assigned as highly intact compared to the signature of sample B and sample C and this could be a marker of (mostly) intact PbS QDs.

4.4.2 Photothermal influence on PbS QDs degradation

The time series, see Figure 4-4 indicate that low power illumination induced no degradation artifacts. Further, the influence of the laser power on the spectral behavior was studied to figure out if a higher power density shows an increase of the "photomarker-signals" Pb-(sulf)oxide. The spectra were background subtracted as mentioned in section 4.3 and normalized to the strong signal peak at 196 cm^{-1} for a better comparison (non-corrected spectra, see appendix 6.5, Figure 6-6). The laser power to measure the photothermal influence of samples A, B and C were increased in six steps from 0.15 mW to 2.0 mW at the same sample spot.

The increase of the relative intensity does not scale linearly with the laser power. With increasing the laser power, the detected Raman signal decreases slightly. The signal decrease can be addressed to SERStrate since the gold evaporated structure reacts very sensitively of heating effects.

Sample A (Figure 4-9a) shows under high-power near-resonant illumination no sign of further degradation, in the measured spectral range from 150 cm^{-1} to 1000 cm^{-1}. This indicated excellent reproducibility and thus a chemical stability of PbS QDs. Consequently, sample A was well sealed. When the PbS mode at 196 cm^{-1} is strong, sharp and the relative intensity of this peak is high in comparison to the region of 250 cm^{-1} and 380 cm^{-1} less degradation occurred and vice versa. It can be concluded that the range between the peak at 196 cm^{-1} and 460 cm^{-1} is a first signal of the degradation state. The sample stability during the whole measurement demonstrated a brilliant sealing and good conditions during the preparation in the glovebox. Improvements to reduce the oxygen contents in sample A could be realized with a dehydration solvent and a reduction of the oxygen content in the glovebox during the synthesis process of PbS QDs.

The band intensities vary during the power measurement in sample B (Figure 4-9b) in the low wave region (196 cm^{-1}, 235 cm^{-1} and 312 cm^{-1}). The peaks at 235 cm^{-1} and 312 cm^{-1} show a clear decrease in the relative band intensities whereby the variation was in the range of the noise measurement. The study of the photothermal oxidation indicated clearly the prominent oxidation peaks at 612 cm^{-1} and also the new upcoming

peak at 980 cm^{-1}. The peak appeared the first time at 980 cm^{-1} when the laser power was above 0.15 mW. The peak belongs to degradation product $PbSO_4$. According to literature PbS oxidized to $PbSO_4$.[16,23,62]

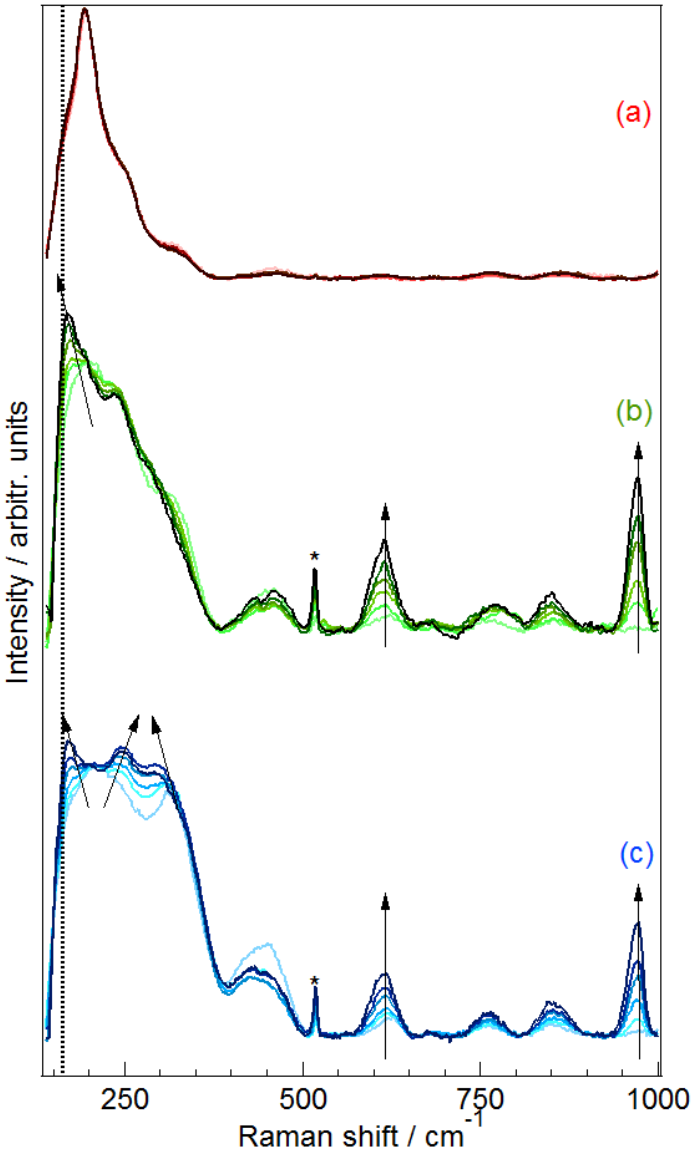

Figure 4-9: Power-dependent degradation on PbS QD/Au. Sample A (a), sample B (b) and sample C (c) were background subtracted and normalized to the peak at 196 cm-1. The power was increased in six steps from 0.15 mW to 2.0 mW with 10 s integration time. The arrows show the direction of spectral changes (blue or redshift). The dotted line presents the dichroitic-filter cut-off at 156 cm^{-1}.

Sample C (Figure 4-9c) showed a high variation in band intensities, similar to sample B. The Raman scattering below 200 cm^{-1} is close to the filter cut off at 156 cm^{-1} that made

the assignment for this band quite complicated. The increase of PbS LO mode from 235 cm^{-1} to 255 cm^{-1} with an increasing laser power can be explained by the ingrowth of the sulfoxide bands (blueshift). The peak at 312 cm^{-1} was redshifted could be due to the slowly PbO_2 formation. Figure 4-9b, the reference spectrum of PbO_2 shows a strong signal at 287 cm^{-1}. Burgio et al. assigned detected a Raman signal at 274 cm^{-1} and defined it as Pb-O-Pb overtone.

It was tried to parameterize the complex spectra at 0.15 mW and 2.0 mW for sample A, B and C, see appendix 6.6 (Figure 6-7). The signal to noise was good for the fitting. Nevertheless, the fittings are not suitable. Just with a combination of Gaussian and Lorentzian was it able to fit the data. Also, the full with half maximum (FWHM) changes are lot and were not reproducible. The fitting is complicated due to the overlapped signals. The more oxidized the samples were the gentler was the fitting. Also, complicated was the broadening close to the dichrotic-filter cut-off at 156 cm^{-1}.

The increase of the peak intensity at 196 cm^{-1} for sample B and C (Figure 4-9) cannot be determined with complete certainty due to the approximation of the dichroitic filter cut-off at 156 cm^{-1}. The redshift of the spectra with an increasing oxidation content is explained due to the strong PbS bulk[23,62,25] phonon mode at 144 cm^{-1} as a result of the Pb-(sulf)oxide degradation products. The reference spectrum of PbO_2 (Figure 4-8a) shows a strong and sharp peak in that area, close to the filter cut-off. Therefore the Pb(-sulf)oxide products can be assumed as a reason for the redshift in the sample B and C. The obvious change for sample C (Figure 4-9c) during the power series was the increase of the relative intensity of the peak at 312 cm^{-1} which belongs to Pb(-sulf)oxide and became nearly the same relative intensity as the 196 cm^{-1} region. The oxidation bands at 312 cm^{-1} and 287 cm^{-1} were still prominent with less laser power. With an increased laser power the bands at 614 cm^{-1} and 980 cm^{-1} become prominent markers for photothermal degradation due to the $PbSO_4$.

The photothermal behavior follows the trend that was obtained with the laser powers up to 2.0 mW, see Figure 4-10 shows PbS QDs at different laser powers from 0.15 mW (a) to 2.0 mW (b) to 8.0 mW (c). The fully oxidized sample had grown into the area of the dichroic-filter at 140 cm^{-1} due to the PbO/PbO_2 band. In Figure 4-10c the laser power

was increased up to 8 mW (10 s integration time) to obtained a fully oxidized PbS QDs sample on gold.

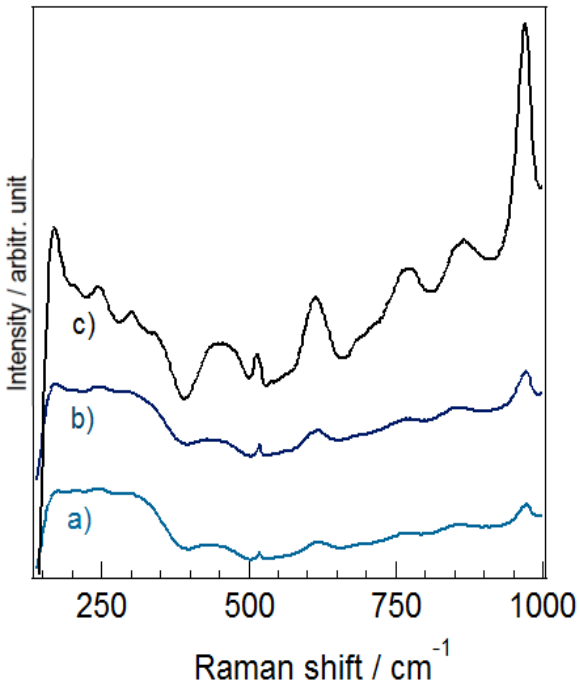

Figure 4-10: The photothermal oxidation of PbS QDs on a SERStrate with a laser power of a) 1.2 mW, b) 2.0mW and c) 8.0 mW. The comparison between the different power spectra indicates the strong increase of the relative intensities of the Pb-(sulf)oxide oxidation products.

The study indicated that trace amounts of oxygen present during PbS QD preparation can be altered by strong electromagnetic fields. The comparison between the sealed samples and the unsealed sample shows the increase of the Pb-(sulf)oxide bands and the PbS phonon modes. The PbS phonon did not allow a qualitative comparison of the O_2-content during the sample preparation due to varying enhancement from SERStrate to SERStrate of from spot-to-spot. But it indicated that for sample A there was less oxygen in the glovebox than in sample B. With a high level of oxygen and/or high laser power the bands at 614 cm^{-1} and 980 cm^{-1} have indicated as oxidation marker. With a low power at 0.15 mW the bands at 196 cm^{-1} and 400 cm^{-1} indicated the trend of the degradation process in PbS QDs.

4.5 Experimental outlook

In this work several challenges have been achieved to develop a reproducible method to detect the degradation behaviour of PbS QDs. The following chapter gives an overview of the next steps in this project to aim a deeper look in the degradation process. This involves the protection of PbS QDs to the ambient conditions and the recording of a completely degradation process.

4.5.1 Characterization of PbS QDs with TERS

The gold evaporated mica glass substrate (Au/mica) covered with a layer of PbS QDs which was used for TER measurement was produced under the same conditions, the same materials and the same synthesis process as the SERS samples.

The quality of one annealed gold substrate (reference) of every produced batch of gold substrates was controlled after every anneling process with STM. The reference showed a formation of big terraces without any dirt and those enable a successful measurement, see Figure 4-11a. Also, the adsorption of PbS QDs was measured with the STM to control the quality of the PbS QD layer. The STM measurement was taken after the TER measurement to avoid any contamination to the sample. Figure 4-11b showed a successfully produced PbS QD sample due to the Au/mica substrate was covered completely with a layer of PbS QDs produced by two SILAR cycles. Furthermore, it was tried to synthesis larger PbS QDs with a higher SILAR cycle number. In Figure 4-11c the PbS QDs were produced by four SILAR cycles. The protocol is the same as for two cycles just the amount of cycles was changed to four SIALR cycles. The comparison between Figure 4-11b and Figure 4-11c shows differences in the size of PbS QDs. With an average size of 10 to 14 nm for two SILAR cycles and 20 nm for four SILAR cycles. Isolated PbS QDs were tried to produce (appendix, Figure 6-8) with those it is possible to record the degradation behavior of a single QDs instead of a sum of PbS QDs as it occurs with a sub-monolayer.

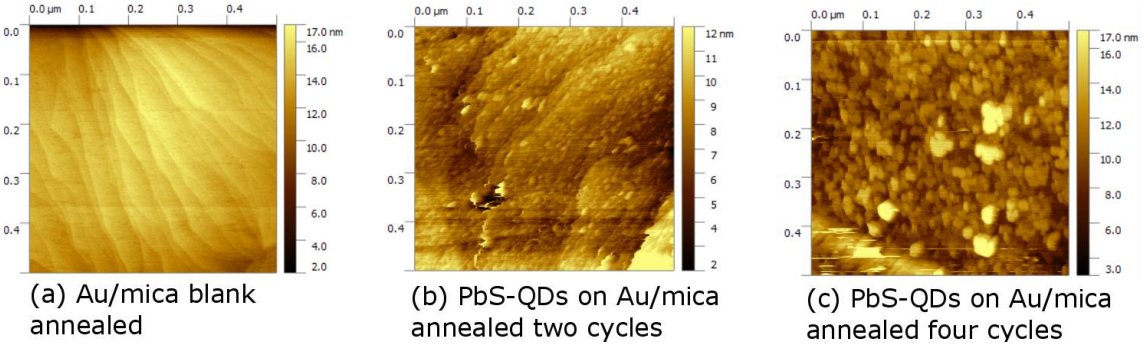

Figure 4-11: a) The reference annealed Au/mica shows terraces and a clean and completely annealed surface. b) The PbS QDs (2xSILAR)/Au/mica covers the surface completely. c) The surface is completely covered from the PbS QDs(4xSILAR) /Au/mica. The STM images were taken from top to bottom with a ScanSpeed of 0.09 s, I-Gain 3.89, P-Gain 1.0, a pixel size of 256 x 256, setpoint of 0.2 V and bias of 0.05 nA.

The TER measurement is illustrated in Figure 4-12. Hereby, the measured PbS QDs were completely oxidized due to the sample was measured for two days and Figure 4-12 shows the measurements of the second day. The results of the measurement from the first day are showed in the appendix 6.7, Figure 6-9 which indicated the SER signature of the LO and 2 LO mode from PbS QDs despite it was measured with TERS. With SEM images of the used gold tip for that measurement it was figured out that the gold tip was benched. Instead of an apex diameter around 20 to 30 nm was the received diameter was 200 nm. With this huge diameter an ensemble of PbS QDs were measured it was not possible to produce a single "*hot spot*". This explains the contained SERS signature instead the TERS signature. TERS measurements are very complex and were influenced by a lot of parameters. The measurement proves the importance of the tip etching process. The etching process is very sensitive and small changes in the position of the gold wire or the etching gold ring can change the corrosion process. It was figured out that the etching machine did not work properly. One of ten prepared gold tips gave a signal related to a TERS signature. A first tip shape control can be done with magnifier and another check with the CMOS camera. The tip should not be benched, the best is a very straight tip. Also, the recorded Raman spectrum can be used to analyze the quality of the tip. A good tip gives a strong enhancement if the tip is approached and give non or very less enhancement if the tip is the retracted for example at 20 nm and 3 µm which is the case in Figure 4-12.

A very good, fast and easy way to characterize the quality of the produced edge tip is the investigation with SEM. The used tip was measured with the SEM after the TER measurement and is illustrated in Figure 4-12. The used tip was a very good tip with a diameter of nearly 20 nm, the etching time was 6.32 min. Good gold tips have an etching time of five to six minutes.

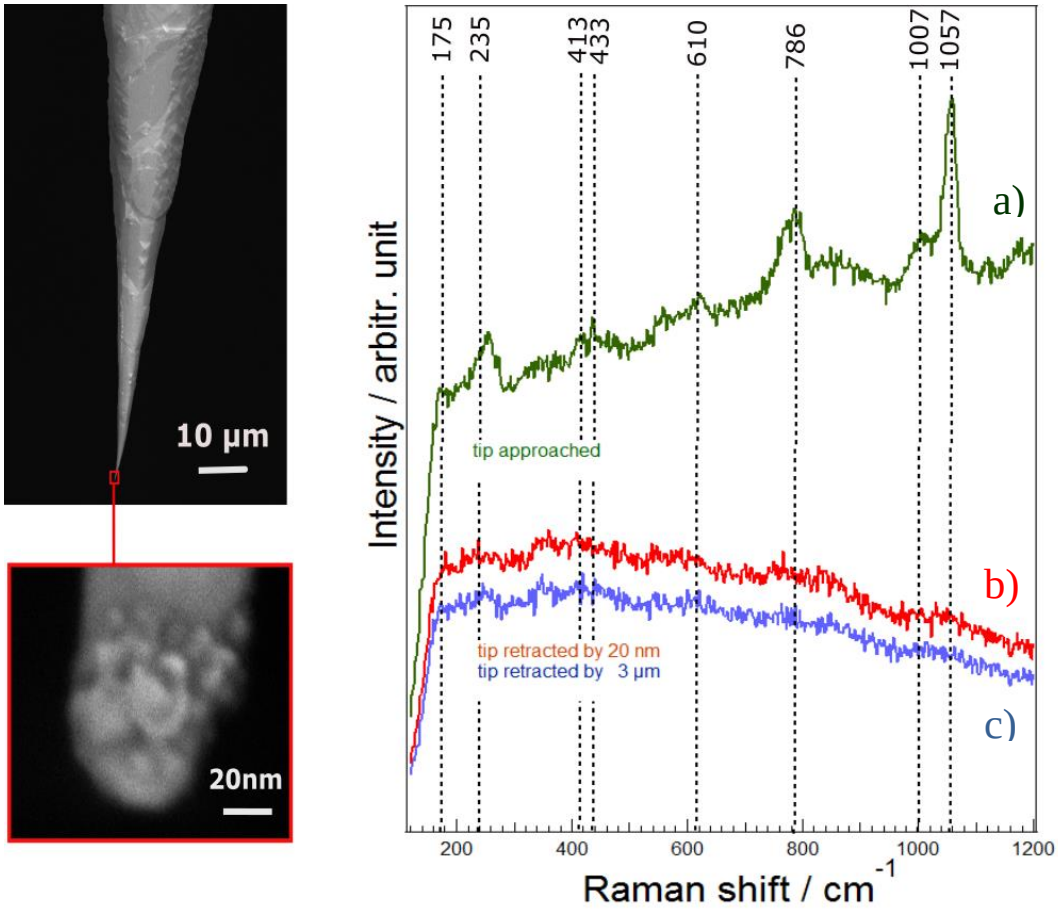

Figure 4-12: PbS QDs / Au measured after one day exposed to oxygen and humidity. The tip is present in a resolution with a scale bar of 10 µm and a zoom in to a scale bar of 20 nm. The retracted tip of TER spectrum of oxidized PbS QDs does not detect a signal with a retraction of 20 nm and 3 µm. After the approach a clear near-field signal is detectable. The signature could belong to a strong oxidized PbS QDs and to impurities on the surface.

The detected spectrum was recorded with a laser power at 1.06 mW and an integration time of 10 s. The measurement shows three different TER Raman spectra obtained with the STM tip in tunneling mode (Figure 4-12a) and retracted 20 nm (Figure 4-12b), and 3 µm (Figure 4-12c) mode. The tunneling mode (approach) gave clear Raman signals at

175 cm^{-1}, 235 cm^{-1}, 413 cm^{-1}, 433 cm^{-1}, 610 cm^{-1}, 786 cm^{-1}, 1007 cm^{-1} and 1057 cm^{-1}. As in detail discussed in section 4.4.1 and 4.4.2 are the peaks at 235 cm-1 related to the PbS LO band, 430 cm^{-1} related to the 2 LO Band and the 610 cm^{-1} related to a $PbSO_4$ oxidation product. If the tip is retracted Raman scattering is not visible.

To mention again the measured PbS QDs sample on Au/mica substrate was already measured with TERS the day before and is highly oxidized. PbS QDs in the SERS study were never being oxidized and illuminated such a long time as the measured PbS QDs with TERS. The sample could also contain impurities.

The signal of the new peaks could be related to nitrate (NO_3) oxidation products (1057 cm^{-1} and 786 cm^{-1}).[63,64,65] It is even possible that the peak at 175 cm^{-1} belongs to the PbS LO mode as well. From section 4.4.2 it is known that a peak at 196 cm^{-1} undergoes a redshift if the oxidation level is high.

In summary, TERS measurements on PbS QD layers are possible, this technique could be an excellent way to analyze the degradation behavior of PbS QDs. With a proper sealing, a short fixation time and isolated PbS QD it can be assumed to detect the full oxidation process of an isolated PbS QD. Next to the characterization of an isolated PbS QDs on Au/mica substrates it is interesting the study the adsorption of PbS QD layers by SILAR process on a porous titanium dioxide (TiO_2). TiO_2 is used in solar cells as carrier material for the sensitizer material. The behavior of PbS QDs can be characterize due to they can be used for QDSSCs. The investigation of all those steps would help to find out the best handling for PbS QDs to produce a photovoltaic device based of PbS QDs with a higher and stable efficiency.

4.5.2 Sealing improvement

PbS QDs are affected by oxygen and humidity one method to protect the material is the sealing in an inert atmosphere. The investigated SER sample B indicated problems with the used sealing process. Little vents which are not observable by eye leaded to a higher oxygen and humidity content. The vents could be possible at the interface between the glass slide and the parafilm and the between the parafilm and the coverslip. Also, for TER measurement a new sealing method is necessary due to the gold tip needs to be in a very close contact to the metal substrate. Therefore, a moveable container to transport

the sample over short distances helps to protect the sample against oxidation. The conditions to create a moveable container belongs to the substrate shape which was 5 x 5 mm^2 for the SERStrate and 15 x 15 mm^2 for the annealed gold substrate for the TER measurement. For SER experiments the preparation of a closed volume with a cover slip was possible. For TER measurements this method was not possible. The distance from the tip to the sample is just few Å.

Therefore, a new transport box, like a container has to develop. The sample in the movable container should be; I) easily changed II) avoid any contact with ambient environment, III) avoid sample flipping.

A container that scales with the diameter of the sample would avoid sample flipping. A gel layer would fix the sample on the same position.

The glass container with a Teflon insert, reach the suitable sample high and is easy to clean with piranha. The sample can be prepared in the glovebox under inert conditions and afterwards it is placed in the Teflon punching and closed with a hermetic cap. The moveable container is just suitable for short distances. During the TER measurement the sample has to be flooded with inert gas. For the flooding a balance has to be found to protect the sample against oxidation and not to disturb the TER measurement.

The advantages are I) the glass container can be easily opened and II) the sample can be taken out of the box with a tweezer. The *"transport box"* is to move the sample from one place to another over a short distance. The sample stage has to be flood with nitrogen or argon to provide inert conditions.

The easy handling of the glass container and the subsequently gently flooding of PbS QDs with argon or nitrogen could be reducing the oxidation before and during the TER measurement.

5 Conclusions

In this thesis the influence of oxygen on the stability of PbS quantum dots is studied and gives a comprehensive overlook on the transformation of crystalline PbS QDs into crystallized oxidation products.

We characterized PbS quantum dots using surface-enhanced Raman spectroscopy (SERS) and tip-enhanced Raman spectroscopy (TERS). These methods allow measuring the Raman scattering even for small amount of samples. We performed the measurements for three samples at different ambient conditions: ranging from an atmosphere nearly absent of oxygen (nitrogen atmosphere) to oxygen content ~21% (air).

The sample measured in nitrogen atmosphere shows a very strong and sharp PbS LO mode at 196 cm^{-1}. This indicates crystalline, mostly intact PbS QDs on that sample. The Raman spectrum of that sample illustrates a peak at 312 cm^{-1}, which corresponds to a small concentration of Pb-(sulf)oxide product and may be due to oxidation during the preparation of the sample. For the sample in an ambient atmosphere with considerable oxygen content, the relative intensity at the peak 196 cm^{-1} decreases and we detect partly formation of crystal PbS in crystal Pb-(sulf)oxide through the Raman line at 312 cm^{-1}. Furthermore, the relative intensities of the Raman signal at 290 cm^{-1}, 312 cm^{-1}, 430 cm^{-1} and 460 cm^{-1} indicates formation of Pb-(sulf)oxide and overlapped with the 2 LO mode of PbS QDs. The photo oxidation induced a new oxidation peak at 980 cm^{-1} that belongs to lead sulfoxide. With an ongoing oxidation the bands at 614 cm^{-1} and 980 cm^{-1} turns out as oxidation marker of $PbSO_4$. This study figured out the oxidation products of PbS QDs and indicate degradation marker of Pb-(sulf)oxide and $PbSO_4$ in comparison to non-oxidized PbS QDs.

As next step the time dependent degradation of an isolated PbS QD could be analyzed with TERS. For that purpose, a suitable sealing method for the TERS experiment has to be developed. With the investigation of isolated QDs the oxidation rate can be understood. This will be useful for the understanding and improvement of photovoltaic devices based on PbS QDs.

6 Appendix

6.1 Determination of variations on SERS substrates

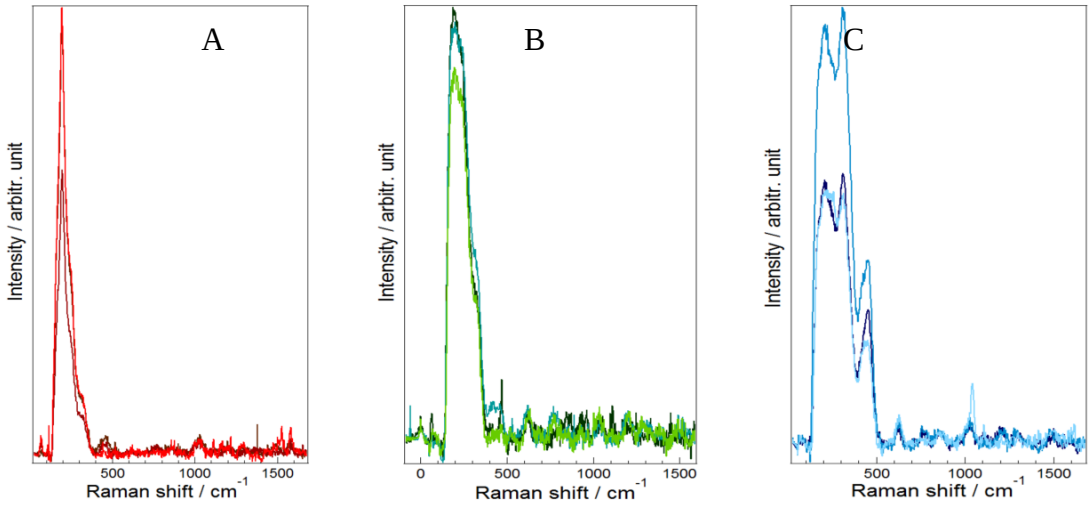

Figure 6-1: The spot to spot variation of sample A, B and C was calculated to analyze the variations of relative intensities within a SERS substrate (SERStrate). Three different spots of one SERS substrate were normalized to peak XY for each sample. The relative peak intensity of peak 196 cm^{-1} was compared to peak 240 cm^{-1} and the average of the three spots were calculated.

6.2 Detection of PbS QDs on gold with SEM and EDX

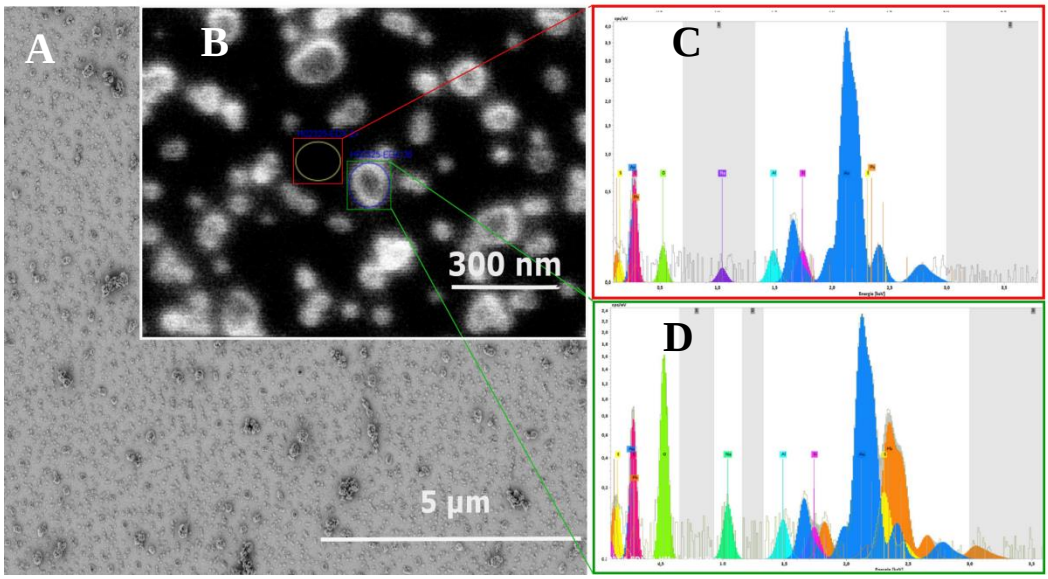

Figure 6-2: A sample of PbS QDs adsorbed on a gold evaporated glass substrate was measured. A) The SEM measurement indicates an adsorbed material on the gold surface, scale bar 5 micron. B) A zoomed in area of this sample, with a scale bar of 300 nm was measured with EDX. C) The EDX measurement did not detect a signal on lead or sulfide on the black measured area, which is red framed D) The EDX measurement indicated the presence of PBS QDs on Au/mica substrates illustrated with the green frame around the white spot.

Element	Ord. Z.	Netto	Masse [%]	Masse Norm. [%]	Atom [%]	abs. Fehler [%] (1 sigma)	rel. Fehler [%] (1 sigma)
Kohlenstoff	6	557	1,27	1,22	12,31	0,37	28,93
Sauerstoff	8	1251	2,90	2,80	21,15	0,64	22,17
Gold	79	6108	65,67	63,48	38,94	3,57	5,44
Aluminium	13	68	0,22	0,22	0,96	0,06	26,38
Silizium	14	100	0,72	0,69	2,98	0,12	16,56
Schwefel	16	227	1,70	1,64	6,19	0,20	11,70
Blei	82	1974	30,98	29,95	17,46	1,98	6,40
		Sum	**103,45**	**100,00**	**100,00**		

Figure 6-3: Elementary analysis of PbS QD on Au/mica substrate. The element table of the EDX analysis showed in Figure 6-3 indicates a higher ratio of lead in comparison to sulfide. One reason is the overlap on the signal at 2.4 keV. Another reason could be the possibility of a lead layer around the particle and the limitation of the EDX as a surface method thus cannot detect the inside of the QD. Therefore, a better alternative for the determination of the atom ration could be SIMS, which is able to cut a part of the QD away and to analyze the “real” ratio of PbS QDs.

6.3 Detection PbS QDs on Au with AFM

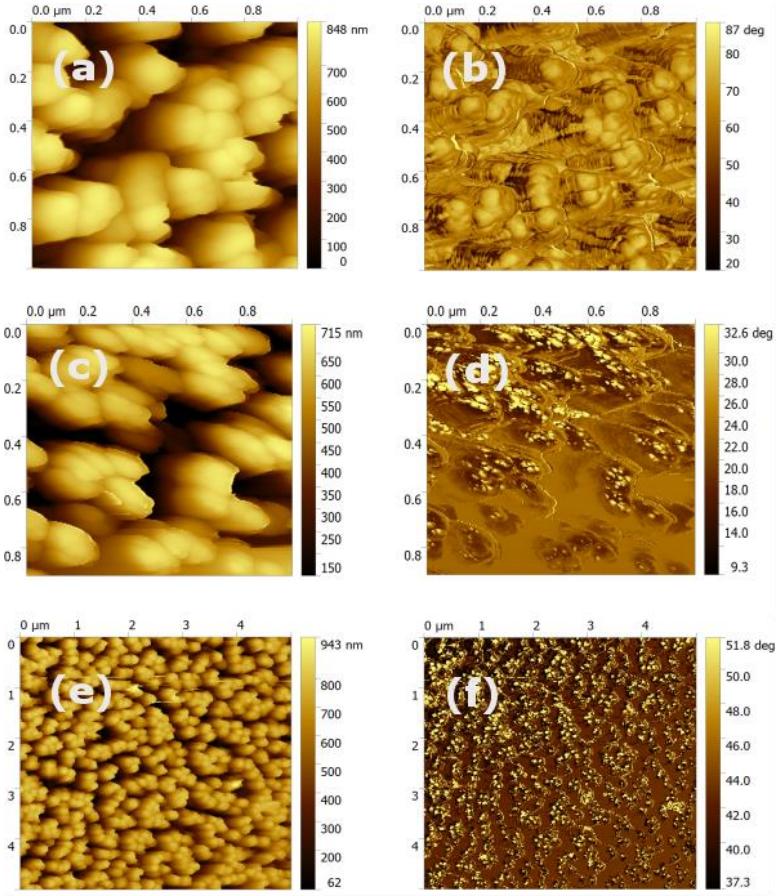

Figure 6-4: PbS QDs on the SERStrate substrate nanopillars were measured on three different spots with AFM in the tipping mode. The three measured spots are present in topographic mode (a),(c),(e) and in the phase contrast mode (b),(d),(f). Spot one (a,b) showed a nanopillar structure. It seems like no detection of the PbS QDs. The absence of PbS QDs could be a sign for submonolayers of PbS QDs. Spot two (c,d) showed the nanopillars and the bright dots in the phase contrast mode which could be PbS QDs. Spot three showed a 5 micron zoom out area of the sample. Whereby, the topographic indicated the nanopillar structure and the white dots on the phase contrast mode could be PbS QDs. The sample is a bit tilted which belongs to the fixation from the sample on the sample holder.

6.4 SER measurement with λ_{ex}= 785 nm

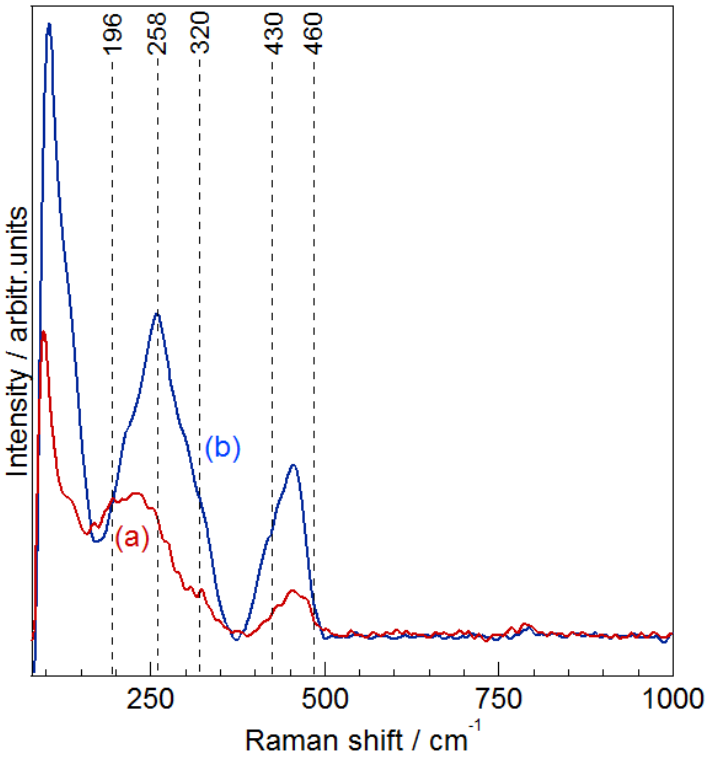

Figure 6-5: The spectra of PbS QDs on SERStrate were recorded with an excitation of λ_{ex}= 785 nm. The measurements showed the same trend for samples a) A and b) C as with the excitation of λ_{ex}= 632.8 nm. The discussed PbS QDs band positions in 4.3 are assigned with dotted lines. The spectra were recorded with an integration time of 10 s, two accumulations with a laser power of 1 mW.

6.5 Raw data of power series measured with SERS

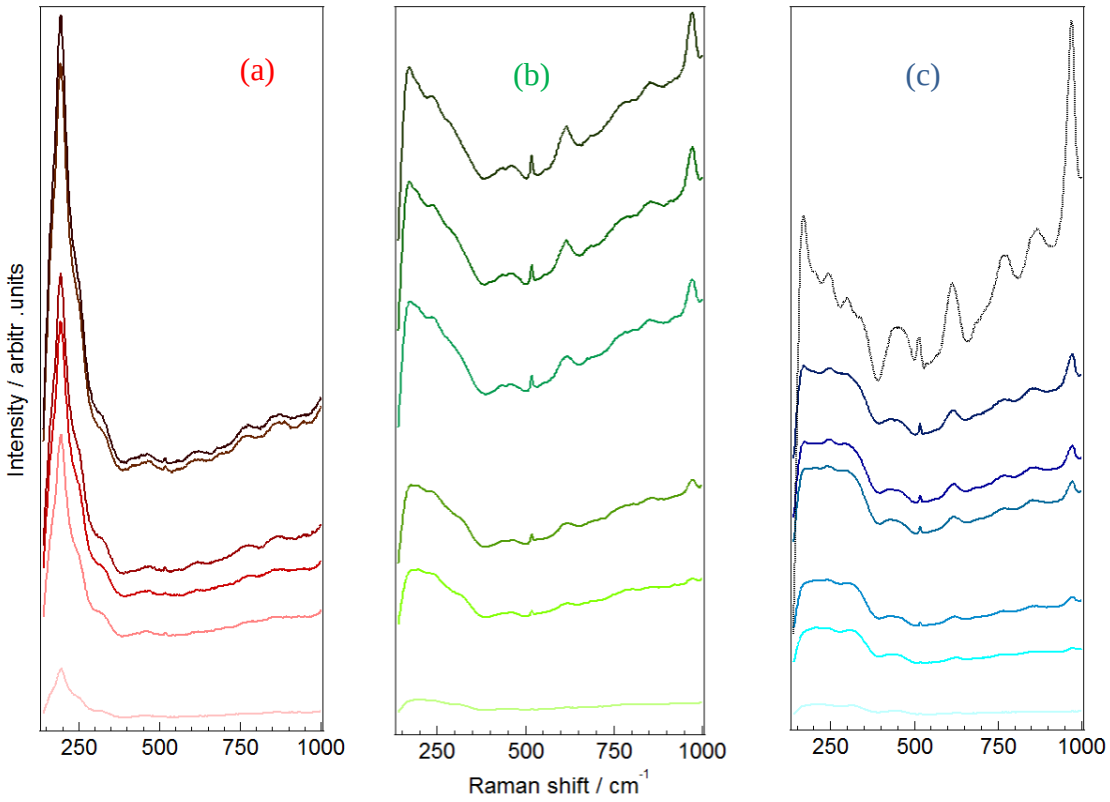

Figure 6-6: Raw, non-background subtracted data of PbS QDs on SERStrate which were contained from a measurement at different laser powers (power series). The power series were recorded at three spots for each sample. Whereby, one of those three spots of each sample is showed in Figure 6-6. For sample (a) A, sample (b) B and sample (c) C the laser power were increased in 6 steps from 0.15 mW to 2.0 mW with 10 s integration time. c) Sample C included an further increase of laser power up to 7 mW to obtained a completely photo-oxidized PbS QD sample.

6.6 SERS peak fitting of measured PbS QDs samples

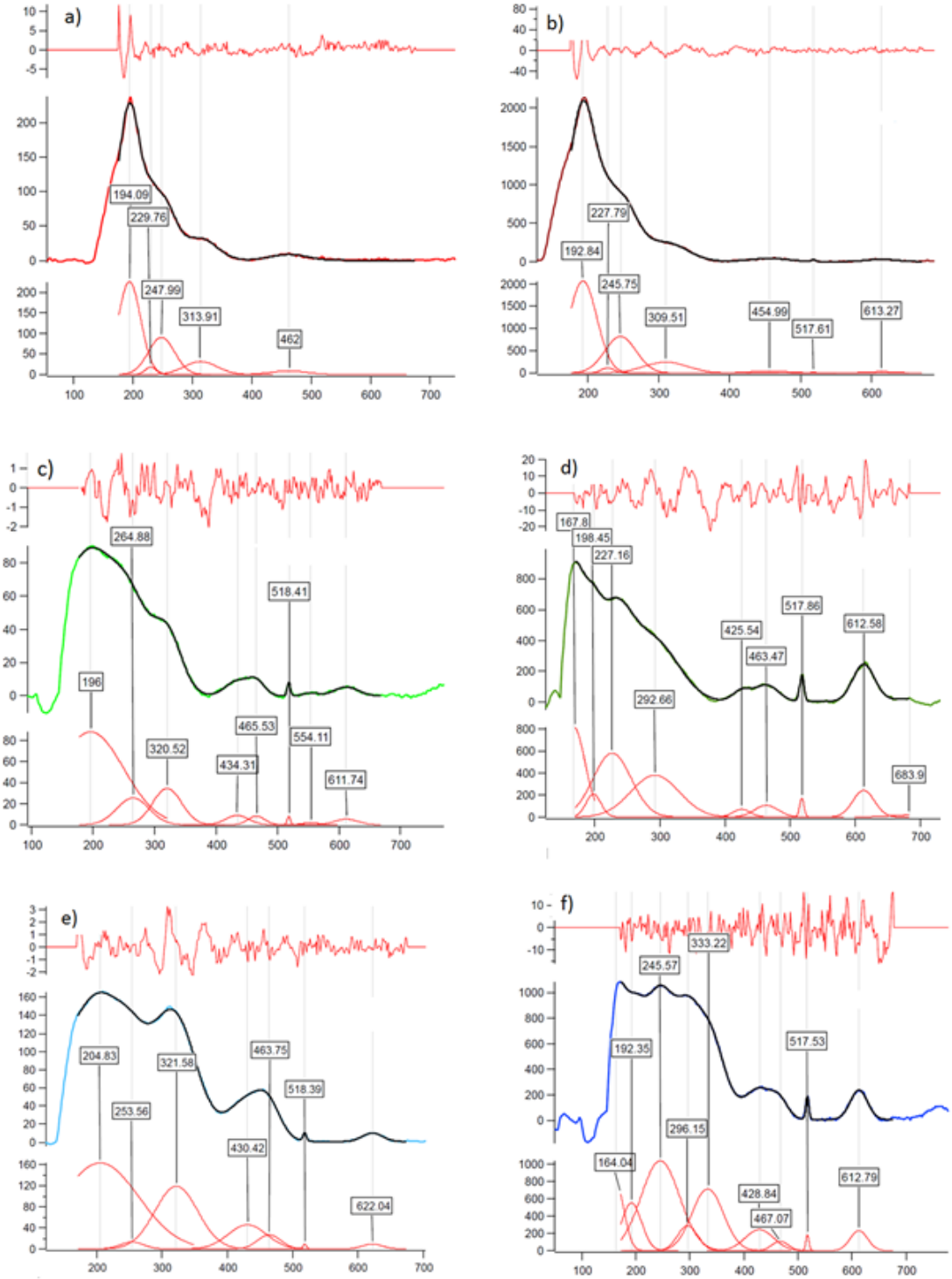

Figure 6-7: The background fitting of SERS spectra was not easy to handle with a mathematical function or a combination of mathematical functions due to the overlapping signals from oxidation products. It was tried to parameterize the resulting spectra with Gaussian and Lorentzian functions. The fitting of the broad peaks shifted between 3-10 wavenumbers. Sample a) A, c) B and e) C showed the fitted spectra which were recorded with a laser power at 0.15 mW. Sample b) A, sample d) B and sample f) C showed the fitted spectra which were recorded with a laser power at 2.0 mW).

6.7 STM and TER measurements of PbS QDs

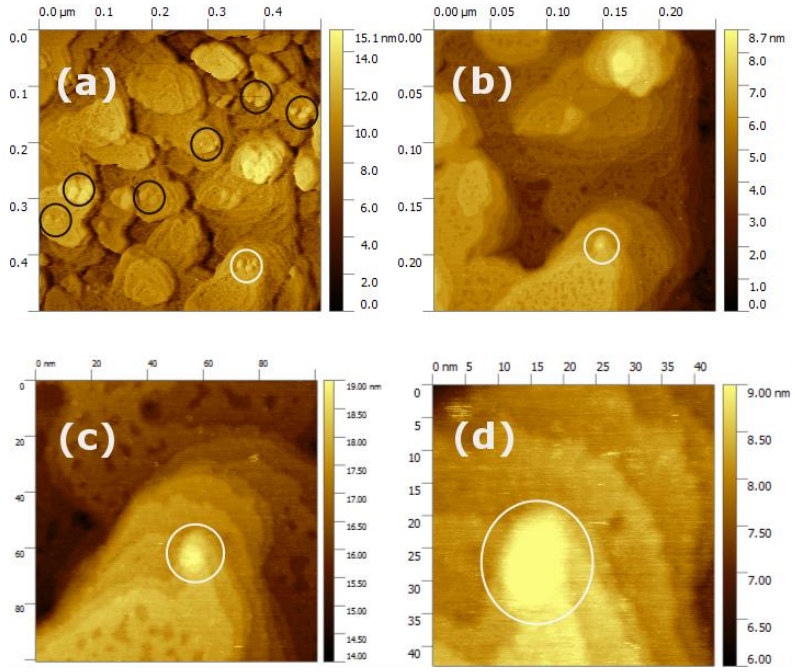

Figure 6-8: With a modification in the SILAR protocol it was possible to produce isolated PbS QDs. The precursor immersion time was changed from 20 s to 15 s and the tipping time was extended from 30 s to 70 s. Further the concentration of the educts was changed from 0.02 to 0.01 M. PbS QDs on gold mica substrate were measured with an STM. The measured area of a) 500 nm showed isolated QDs, which were marked with a black circle. The zoomed in area was marked with a white cycle. b) The first zoom in to 250 nm indicated the reduction of four measured PbS QDs to one QD. The further zoom in was sown to c) 100 nm and d) 45 nm. The single QD has a diameter of 10 to 15 nm. The scanning direction was from bottom to top (a and b: ScanSpeed 1/I-Gain 3.2/ P-Gain 1.0/ Pixel 256 x 256/ Setpoint 0.2 V, bias 0.05mA), (c and: ScanSpeed 1.2/I-Gain 3.2/ P-Gain 1.0/ Pixel 256 x 256/ Setpoint 0.5, bias 0.04 mA) With the measurement of a single QD a detection of an overlay of several QDs could be avoid. The production of an isolated PbS QD was successful but the protocol is not reproducible, due to the fact it was tried once.

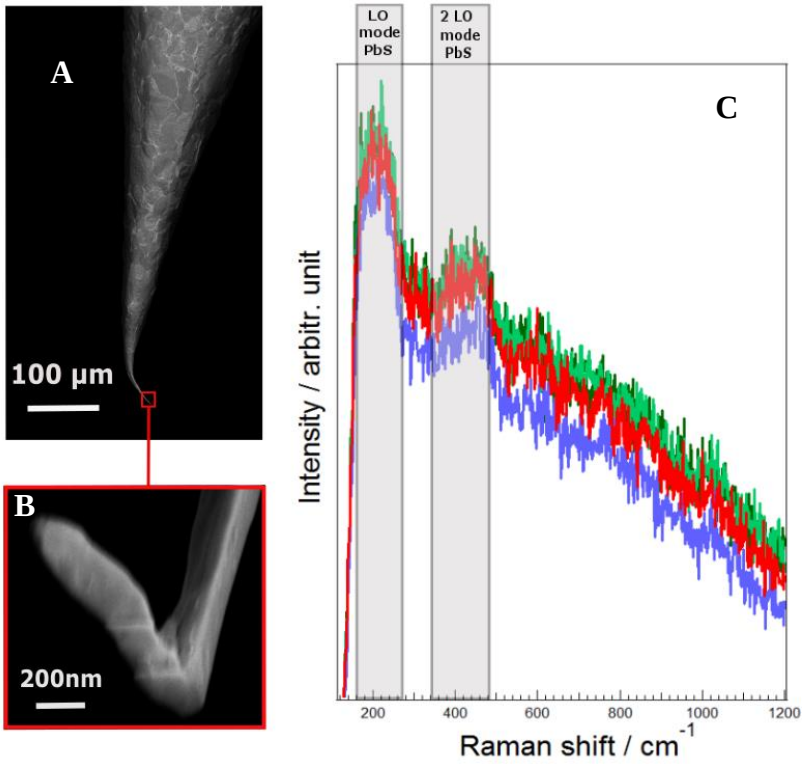

Figure 6-9: A) The used gold tip was bended and B) crashed after the TER measurement. Nevertheless, the scale bar at 200 nm shows that the end of the tip was around 150 nm and therefore too huge to produce a good "*hot spot*". C) The PbS QD sample which measurement with TERS, as reported in chapter 4.5.1 is showed at the first day of measurement. Clearly the LO and 2 LO mode of PbS-QDs is recorded. The signal was measured with 0.86 mW and 10 s integration time.

List of figures

Bibliography

1. Parida, B., Iniyan, S. & Goic, R. A review of solar photovoltaic technologies. **15,** 1625–1636 (2011).
2. Tian, J. & Cao, G. Semiconductor quantum dot-sensitized solar cells. **1,** 1–8 (2013).
3. Tsao, J., Science, B. E., Lewis, N. & Crabtree, G. Solar FAQs. 1–24 (2006).
4. Chen, H. & Wong, K. Donor-acceptor small molecule with coplanar and rigid π - bridge for efficient organic solar cells. (2016). doi:10.1016/j.solmat.2012.10.019
5. Bisquert, J. Breakthroughs in the Development of Semiconductor- Sensitized Solar Cells *. 3046–3052 (2010). doi:10.1021/jz100863b
6. Ru, S. ScienceDirect Tabulated values of the Shockley – Queisser limit for single junction solar cells. **130,** 139–147 (2016).
7. Wise, F. W. Lead Salt Quantum Dots : the Limit of Strong Quantum Confinement. 773–780 (2000).
8. Veggel, F. C. J. M. Van. Near-Infrared Quantum Dots and Their Delicate Synthesis, Challenging Characterization, and Exciting Potential Applications. (2014).
9. Graetzel, M., Janssen, R. A. J., Mitzi, D. B. & Sargent, E. H. Materials interface engineering for. (2012). doi:10.1038/nature11476
10. Pattantyus-abraham, A. G. *et al.* Depleted-Heterojunction Colloidal. **4,** 3374–3380 (1800).
11. Donega, C. D. M. Synthesis and properties of colloidal heteronanocrystals w. 1512–1546 (2011). doi:10.1039/c0cs00055h
12. Xu, J. *et al.* Colloidal Nanocrystal-Based Light-Emitting Diodes Fabricated on Plastic – Towards Flexible Quantum Dot Optoelectronics a) b). **2,** 1–2 (2009).
13. Wood, B. V. *et al.* Inkjet-Printed Quantum Dot – Polymer Composites for Full-Color AC-Driven Displays. 2151–2155 (2009). doi:10.1002/adma.200803256
14. Ning, Z. *et al.* Air-stable n-type colloidal quantum dot solids. **13,** 4–10 (2014).
15. Batonneau, Y., Bremard, C., Laureyns, J. & Merlin, J. C. Microscopic and imaging Raman scattering study of PbS and its photo-oxidation product. **31,** 1113–1119 (2000).
16. Blackburn, J. L., Chappell, H., Luther, J. M., Nozik, A. J. & Johnson, J. C. Correlation between photooxidation and the appearance of raman scattering bands in lead chalcogenide quantum dots. *J. Phys. Chem. Lett.* **2,** 599–603 (2011).
17. Ihly, R., Tolentino, J., Liu, Y., Gibbs, M. & Law, M. The Photothermal Stability of PbS Quantum Dot Solids. 8175–8186 (2011).
18. Peterson, J. & Krauss, T. D. Photobrightening and photodarkening in PbS quantum dots w. 3851–3856 (2006). doi:10.1039/b604743b

19. Rogach, A. L., Eychmüller, A., Hickey, S. G. & Kershaw, S. V. reviews Infrared-Emitting Colloidal Nanocrystals : Synthesis , Assembly , Spectroscopy , and Applications. 536–557 doi:10.1002/smll.200600625

20. Ip, A. H. *et al.* Hybrid passivated colloidal quantum dot solids. **7,** (2012).

21. Chuang, C. M., Brown, P. R., Bulović, V. & Bawendi, M. G. Improved performance and stability in quantum dot solar cells through band alignment engineering. **13,** (2014).

22. Search, H., Journals, C., Contact, A., Iopscience, M. & Address, I. P. Resonance effects in Raman scattering of quantum dots formed by the Langmuir-Blodgett method. **012045,**

23. Batonneau, Y. & Br, C. Microscopic and imaging Raman scattering study of PbS and its photo-oxidation products. **1119,** 1113–1119 (2017).

24. Smith, G. D., Firth, S., Clark, R. J. H. & Cardona, M. First- and second-order Raman spectra of galena (PbS). *J. Appl. Phys.* **92,** 4375–4380 (2002).

25. Baranov, a. V. *et al.* Comparative analysis of Raman spectra of PbS macro- and nanocrystals. *Opt. Spectrosc.* **109,** 268–271 (2010).

26. Bumbrah, G. S. & Sharma, R. M. Raman spectroscopy – Basic principle , instrumentation and selected applications for the characterization of drugs of abuse. *Egypt. J. FORENSIC Sci.* (2015). doi:10.1016/j.ejfs.2015.06.001

27. Smith, E. & Dent, G. *Modern Raman Spectroscopy A Pratical Approach*. (John Wiley & Sons, Ltd, 2005).

28. Freude, D. *Molekülphysik*. **2,** (2006).

29. Ru, E. C. Le & Etchegoin, P. G. *Principles of Surface-Enhanced Raman Spectroscopy and related plasmonic effects*. (Elsevier B.V., 2009).

30. Spectroscopy, M. R. *et al.* Raman Selection Rules TERS group meeting Vibration in molecules : normal modes. (2014).

31. Ren, B., Picardi, G. & Pettinger, B. Tip-Enhanced Raman Spectroscopy of Benzenethiol Adsorbed on Au and Pt Single-Crystal Surfaces**. *Anal. Surf.* 139–142 (2005). doi:10.1002/anie.200460656

32. Raman, C. V. & Krishnan, K. . A New Typ of Secondary Radatiaiton. *Nature* (1928).

33. Domke, K. F. Tip-enhanced Raman spectroscopy – Topographic and chemical information on the nanoscale. *Pharmazie* (2006).

34. Kopie von subito e.V., geliefert für Westfälische Wilhelms Universität Münster (HSL14X01282).

35. oyce Y. Wong, Joseph D. Bronzino, D. R. P. *Biomaterials: Principles and Practices*. (CRC Press, 2013).

36. Sprafke, A. N. Optische Nahfeld-Wechselwirkungen von Plasmonen mit ihrer Umgebung. (2014).

37. Schlücker, S. Surface-enhanced raman spectroscopy: Concepts and chemical applications. *Angew. Chemie - Int. Ed.* **53,** 4756–4795 (2014).

38. Oberlander, E. & Photonik, B. Raman-Spektroskopie in Biomedizin und an nahfeldgekoppelten Nanosystemen. (2016).

39. Fleischmann, M., Hendra, P. J. & McQuillan, A. J. Raman spectra of pyridine adsorbed at a silver electrode. *Chem. Phys. Lett.* **26,** 163–166 (1974).

40. Jeanmaire, D. L. & Van Duyne, R. P. Surface raman spectroelectrochemistryPart I. Heterocyclic, aromatic, and aliphatic amines adsorbed on the anodized silver electrode. *J. Electroanal. Chem.* **84,** 1–20 (1977).

41. A. Otto, I. Mrozek, H. Grabhorn, W. A. Surface-enhanced Raman Scatttering. *J. Phys. Condens. Matter* **4,** 1143 (1992).

42. Schmidt, M. S., Hübner, J. & Boisen, A. Large area fabrication of leaning silicon nanopillars for Surface Enhanced Raman Spectroscopy. *Adv. Mater.* **24,** 11–18 (2012).

43. Fan, M., Andrade, G. F. S. & Brolo, A. G. Analytica Chimica Acta A review on the fabrication of substrates for surface enhanced Raman spectroscopy and their applications in analytical chemistry. *Anal. Chim. Acta* **693,** 7–25 (2011).

44. Blum, C. *et al.* Understanding tip-enhanced Raman spectra of biological molecules: A combined Raman, SERS and TERS study. *J. Raman Spectrosc.* **43,** 1895–1904 (2012).

45. Anderson, M. S. Locally Enhanced Raman Spectroscopy with an Atomic Force Microscope. *Appl. Phys. Lett.* **76,** 3130–3132 (2000).

46. Zhang, Z., Sheng, S., Wang, R. & Sun, M. Tip-Enhanced Raman Spectroscopy. doi:10.1021/acs.analchem.6b02093

47. Demming, F., Jersch, J., Dickmann, K. & Geshev, P. I. Calculation of the field enhancement on laser-illuminated scanning probe tips by the boundary element method. *Appl. Phys. B Lasers Opt.* **66,** 593–598 (1998).

48. Hess, Ortwin, E. G. No TitPhotonics of Quantum-Dot Nanomaterials and Devices le. (2011).

49. Hambrock, D. J. Nichtwässrige Nano-Kolloide Metallorganischen Precursoren Dissertation zur Erlangung der Doktorwürde der Fakultät für Chemie der Ruhr-Universität Bochum. (2003).

50. Yee, C. & Yee, C. Development of Low Temperature , Aqueous Synthesis Method of Lead Sulfide Quantum Dots. (2014).

51. Kang, I. & Wise, F. W. Electronic structure and optical properties of PbS and PbSe quantum dots. **14,** 1632–1646 (1997).

52. Group, R., Division, S. & Berkeley, L. Materials Availability Expands the Opportunity for Large-Scale Photovoltaics Deployment. **43,** 2072–2077 (2009).

53. Pathan, H. M. & Lokhande, C. D. Deposition of metal chalcogenide thin films by successive ionic layer adsorption and reaction (SILAR) method. **27,** 85–111 (2004).

54. Wang, H., Barceló, I., Lana-villarreal, T., Gómez, R. & Bonn, M. Supporting Information for Interplay Between Structure , Stoichiometry and Electron Transfer Dynamics. 1–16

55. Kraus, S., Mainz, J. G. & Planck, M. Epitaxial Growth of Quantum Dots by Successive Ionic Layer Adsorption and Reaction. (2013).

56. Nanda, K. K., Sahu, S. N., Soni, R. K. & Tripathy, S. Raman spectroscopy of PbS nanocrystalline semiconductors. *Phys. Rev. B* **58,** 405–407 (1998).

57. Krauss, T., Wise, F. & Tanner, D. Observation of Coupled Vibrational Modes of a Semiconductor Nanocrystal. *Phys. Rev. Lett.* **76,** 1376–1379 (1996).

58. Krauss, T. D. & Wise, F. W. Raman-scattering study of exciton-phonon coupling in PbS nanocrystals. *Phys. Rev. B* **55,** 9860–9865 (1997).

59. Clark, R. J. H., Cridland, L., Kariuki, B. M., Harris, K. D. M. & Withnall, R. Svnthesis, Structural Characterisation and Raman Spectroscopy of the Inorganic Pigments Lead Tin Yellow Tvpes I and II and Lead Antimonate Yellow: Their Identification on Medieval Paintings and Manuscripts. (1995).

60. Burgio, L., Clark, R. J. & Firth, S. Raman spectroscopy as a means for the identification of plattnerite (PbO2), of lead pigments and of their degradation products. *Analyst* **126,** 222–227 (2001).

61. Burgio, L. & Clark, R. J. H. *Library of FT-Raman spectra of pigments , minerals , pigment media and varnishes , and supplement to existing library of Raman spectra of pigments with visible excitation*. **57,** (2001).

62. Shapter, J. G., Brooker, M. H. & Skinner, W. M. Observation of the oxidation of galena using Raman spectroscopy. *Int. J. Miner. Process.* **60,** 199–211 (2000).

63. So, N. *et al.* Vibrational Studies of. **2,** 981–989 (2009).

64. Chan, C. K., Flagan, R. C. & Seinfeld, J. H. Resonance Structures in Elastic and Raman-Scattering From Microspheres. *Appl. Opt.* **30,** 459–467 (1991).

65. Cram, A. G. & Davies, M. B. A Raman and IR Spectrophotomeric Study of some Basic Lead Nitrate Componds and their Thermal Decompostion Produckts. **38,** 1111–1117 (1976).

Acknowledgment

I would like to express my sincerest thanks to Dr. Katrin F. Domke for her tremendous support and guidance during my work also for the offering to write my master thesis in her research group at the Max-Planck-Institute. My sincere thanks also go to PD Dr. Markus Braun for his support, guidance and constructive feedbacks. Thank you to both for the inspiring discussion and critical comments.

I would also like to thank Prof. Dr. Josef Wachtveitl for being the second reviewer.

I would also like to thank Natalia and Amala for their great assistance and for my formal introduction to the research in PbS quantum dots.
I also wanna thank Helma Burg for her effort on the AFM and Gunnar Glasser, who took the SEM pictures.

My deepest thanks address to my friend Farah. I cannot thank you enough for your help and your way you calm me down. I would like to express my thanks also to Jenee, Anja, Christine and Sonay. I´m impressed and I´m proud to call you friends.

Finally, I would like to express my deepest gratitude to my family for supporting and advising me during this work and to Julien who drives me crazy and gives me a smile every day.

Declaration of authorship

I hereby declare that the thesis submitted is my own unaided work. All direct or indirect sources used are acknowledged as references.

I am aware that the thesis in digital form can be examined for the use of unauthorized aid and in order to determine whether the thesis as a whole or parts incorporated in it may be deemed as plagiarism. For the comparison of my work with existing sources I agree that it shall be entered in a database where it shall also remain after examination, to enable comparison with future theses submitted. Further rights of reproduction and usage, however, are not granted here.

_____ Mainz, October 27th 2016

First and last name city, date